รายงานการวิจัยฉบับสมบรูณ์ปีที่ 1

การพัฒนา การศึกษาคุณสมบัติ และการประยุกต์ใช้ ของถ่านกัมมันต์ที่ได้จาก แบคทีเรียเซลลูโลส

Development and characterization of activated carbon derived from bacterial cellulose

(สัญญาเลขที่ GB-A_60_035_21_06)

แหล่งทุน ทุนอุดหนุนการวิจัยจากเงินรายได้ ประเภทเงินอุดหนุนการวิจัยจากรัฐบาล ประจำปีงบประมาณ 2560

หัวหน้าโครงการ ศาสตราจารย์ ดร.เหมือนเดือน พิศาลพงศ์

ส่วนงาน ภาควิชาวิศวกรรมเคมี คณะวิศวกรรมศาสตร์

กิตติกรรมประกาศ

โครงการวิจัยนี้ได้รับทุนอุดหนุนการวิจัยจากจุฬาลงกรณ์มหาวิทยาลัยและสำนักงานคณะกรรมการ วิจัยแห่งชาติ (วช.) นอกจากนี้ ผู้วิจัยขอขอบคุณ นายธัชดนัย อัศวมงคลกุล และ นายเธียรพิเชฐ เพิงใหญ่ นิสิตในที่ปรึกษาซีเนียร์โปรเจ็ค (Senior Project), นายมิฟตะห์ฟาริด อิบนุอับดุลวาฮับ นิสิตในที่ปรึกษาวิทยานิพนธ์ระดับปริญญาโท และ นายอานนท์ ขำแก้ว นิสิตในที่ปรึกษาวิทยานิพนธ์ระดับปริญญาเอก ภาควิชา วิศวกรรมเคมี คณะวิศวกรรมศาสตร์ จุฬาลงกรณ์มหาวิทยาลัย ที่มีส่วนสำคัญในการช่วยในการดำเนินการทดลองวิจัย อีกทั้งขอขอบคุณ การสนับสนุนจากทุน “100 ปี จุฬาลงกรณ์มหาวิทยาลัย” สำหรับทุนอุดหนุนการศึกษาสำหรับนิสิตระดับปริญญาเอก

Acknowledgement

This Research is funded by Chulalongkorn University and the National Research Council of Thailand (NRCT). I would like to thank my senior project advisees, Mr. Tatdanai Asavamongkolkul and Mr. Tianpichet Perngyai; my Master’s thesis advisee, Mr. Miftahfarid Ibnu Abdulwahab; and my Doctoral thesis advisee, Mr. Arnon Khamkeaw for their assistances in research works. I also would like to acknowledge the 100th Anniversary Chulalongkorn University Fund for doctoral scholarship.

บทคัดย่อ

แบคทีเรียเซลลูโลส (BC) ได้ถูกนำมาศึกษาเพื่อใช้เป็นวัสดุใหม่สำหรับการเตรียมถ่านกัมมันต์ โดยผ่านกระบวนการทำแห้ง และกระบวนการกระตุ้นทางเคมีด้วยการใช้สารละลายกรดฟอสฟิวริค (H_3PO_4) เป็นตัวกระตุ้น ที่อุณหภูมิ 400, 500 และ 600 องศาเซนติเกรด สมบัติของถ่านกัมมันต์ ถูกวิเคราะห์ตรวจสอบ เช่น คุณสมบัติทางเคมี, โครงสร้าง และ ลักษณะรูพรุน คุณสมบัติทนความร้อน ด้วยเครื่อง Fourier transform infrared spectroscopy (FT-IR), X-ray diffraction (XRD), N_2 -physisorption (BET), scanning electron microscopy (SEM) , thermal gravimetric (TGA) จากการทดลองพบว่า ถ่านกัมมันต์จาก BC ที่ได้จากการถูกกระตุ้นที่ 500 องศาเซนติเกรด (BC-AC500) มีพื้นที่ผิวที่วิเคราะห์โดยBET สูงสุดที่ 1,734 ตารางเมตร/กรัม โดยมีโครงสร้างรูพรุนขนาดกลาง มีขนาดรูพรุนโดยเฉลี่ยเท่ากับ 2.33 นาโนเมตร มีปริมาตรความเพรุนสูงถึง 1.01 ลูกบาศก์เมตร/กรัม สมบัติการดูดซับถูกประเมินโดยใช้เป็นตัวดูดซับเมทิลีนบลู (MB) โดยข้อมูลค่าดูดซับที่สมดุลถูกนำไปวิเคราะห์ด้วยแบบจำลองไอโซเทอมแบบ Langmuir, Freundlich, และ Redlich-Peterson โดยพบว่าข้อมูลการดูดซับที่สมดุลมีความสอดคล้องกับการอธิบายโดยแบบจำลองแบบ Redlich-Peterson มากที่สุด ที่ค่าสัมประสิทธิ์สหสัมพันธ (Correlation coefficient) ที่ค่า $R^2 = 1.0$ มีค่าการดูดซับที่สมดุลสูงสุด (q_m) ที่ 505.8 มิลลิกรัมต่อกรัม ผลจากการทดสอบชี้ให้เห็นว่า ถ่านกัมมันต์จาก BC มีศักยภาพในการนำมาใช้เป็นตัวดูดซับที่มีประสิทธิภาพสูง นอกจากนี้ BC และถ่านกัมมันต์ที่เตรียมจาก BC ได้ถูกพัฒนาต่อไปเป็นตัวรอบรับตัวเร่งปฏิกิริยาตัวเร่งปฏิกิริยาแบบใหม่ Al/BC ถูกเตรียมโดยการแช่ BC บริสุทธิ์ในสภาวะเจลบวมน้ำ (hydrogel) ในสารละลายอลูมิเนียมไนเตรตในน้ำ จากนั้นนำไปทำแห้งและเผาภายใต้อุณหภูมิสูง เมื่อนำไปใช้ในปฏิกิริยาการแยกน้ำออกจากเอทานอล (Ethanol dehydration) ตัวเร่งปฏิกิริยา Al/BC มีสมบัติที่น่าสนใจหลายประการ เช่น มีการกระจายที่ดีของโลหะ มีความเสถียรทางเคมีและความร้อนที่สูง ให้ค่าผลได้ของไดเอทิลอีเทอร์จากเอทานอลสูงที่ประมาณ 42 เปอร์เซ็นต์ ที่อุณหภูมิ 200 องศาเซนติเกรด โดยมีค่าการเลือกเกิด (selectivity) เกือบ 100 เปอร์เซ็นต์ นอกจากนี้ยังได้มีการพัฒนาถ่านกัมมันต์จาก BC ต่อไปเพื่อไปใช้เป็นตัวรองรับของตัวเร่งปฏิกิริยาแบบกรด ในปฏิกิริยาการแยกน้ำออกจากเอทานอล (ethanol dehydration) โดยศึกษาที่อุณหภูมิตั้งแต่ 200 ถึง 400°C

Abstract

Bacterial cellulose (BC) was investigated as a novel material for preparing activated carbons. BC was dried by heating and it was carbonized with a chemical activation process using phosphoric acid (H_3PO_4) as an activating agent at different temperatures (400, 500 and 600 °C). The properties of the activated carbons were characterized such as chemical property, structure, pore size, thermal property by Fourier transform infrared spectroscopy (FT-IR), X-ray diffraction (XRD), N_2 -physisorption (BET), scanning electron microscopy (SEM) , thermal gravimetric (TGA). The obtained BC activated carbons at carbonization temperature of 500 °C (BC-AC500) showed maximum BET surface area (1,734 m^2/g) with mesoporous structure (2.33 nm) and large pore volume (1.01 cm^3/g). The adsorption capacity was evaluated by using as adsorbent for the adsorption of methylene blue (MB). The equilibrium adsorption data were analyzed by the Langmuir, Freundlich, and Redlich-Peterson isotherm models. The results showed that the Redlich-Peterson model was found to be most fitted to the equilibrium data with correlation coefficient (R^2) value of 1.000. The maximum adsorption capacity (q_m) was 505.8 mg/g. The experimental results indicated that the BC activated carbon has the potential to be used as an effective adsorbent. Besides, BC and BC activated carbon has been further developed as catalyst supports. A novel catalyst of Al/BC was developed by soaking purified BC hydrogel in aluminum nitrate aqueous solution, dehydration and calcination. The Al/BC catalyst has many promising properties as catalyst in ethanol dehydration, such as good metal dispersion, high chemical and thermal stabilities. The high yield of diethyl ether at ~ 42 % can be produced from ethanol at 200 °C with the selectivity of almost 100% by using Al/BC as catalyst in ethanol dehydration. In addition, BC activated carbon is continuously developed and applied as acid catalyst in the ethanol dehydration reaction at the temperature from 200-400 °C.

สารบัญเรื่อง (Table of Contents)

สารบัญตาราง (List of Tables)

หน้า

สารบัญภาพ (List of Illustration)

หน้า

1. Introduction

1.1 Motivation

Activated carbon [1] is a form of carbon with high porosity, high surface area with physical and chemical stability, high adsorptive activity and high mechanical strength. Therefore, it is widely used in various applications in the industries such as an adsorbent in pressure swing adsorption [2], catalyst or catalyst support in chemical reactions [3], the removal of heavy metals from wastewaters [4], and gas separation process [5].

Activated carbon is usually derived from coal, wood or petroleum residues [6]. Biomass materials are considered as alternative raw materials which are inexpensive and renewable, such as hazelnut shell [7], coconut shell [8] and many agricultural wastes. Bacterial cellulose (BC) [9] is a cellulosic biomaterial with the formula $(C_6H_{10}O_5)_n$ which is produced by bacteria, *Acetobacter xylinum*. BC has the unique properties including its high tensile strength, high water absorption capacity, high crystallinity and a nano-fiber network. Because of these characteristics, this research has been focusing on activated carbon derived from BC and the characteristics of BC activated carbon were studied.

BC was dried by heating and it was carbonized with a chemical activation process using phosphoric acid (H_3PO_4) as an activating agent at different temperatures (400, 500 and 600 °C). The properties of the activated carbons were characterized by X-ray diffraction (XRD), scanning electron microscopy (SEM), N_2-physisorption, Fourier transform infrared spectroscopy (FT-IR) and thermal gravimetric (TGA). Absorption capacity of BC activated carbon was investigated by using as adsorbent for the adsorption of methylene blue (MB). Novel catalysts using BC and activated carbon derived from BC were developed and characterized by using chemical activation (H_3PO_4 as activated agent) at different activation temperatures such as 400, 500 and 600°C. The physical properties of samples were examined by means of XRD, SEM, N_2-physisorption, FTIR and TGA. In addition, BC activated carbons were used as catalyst support for acid catalysts in ethanol dehydration reaction at various temperatures in range 200 – 400°C.

1.2 Specific objectives of the study

1.2.1 To develop and characterize activated carbons derived from BC

1.2.2 To evaluate absorption capacity of activated carbons derived from BC

1.2.3 To examine the catalytic activities of solid acid catalyst activity in the ethanol dehydration reaction such as selectivity and conversion.

1.3 Theory and literature review

Activated carbon preparation: There are two methods for activated carbon preparation; chemical and physical activation [1, 10-12]. Each of methods is responsible in different characteristics and structure of activated carbon.

- Physical activation: The process is divided into 2 steps. BC will be carbonized first at temperature range of 400-800^{o}C to obtain charcoal and reduce volatile substance. Secondly, charcoal will be followed by activation step by oxygen or stream at temperature range 600-900^{o}C.
- Chemical activation: BC is impregnated with an activating agent and then carbonized under an absence of atmosphere at lower temperature range of 450-600^{o}C. The activating agent is typically acid or basis solution such as $ZnCl_2$, H_3PO_4, NaOH and KOH. The activating agent can partially dissolve the cellulosic components of the sample. This activation needs lower carbonization temperature, obtains higher yield, higher surface area, and better developed porosities compared to the physical activation.

1.3.1 BC activated carbon by impregnation with H_3PO_4 solution

Our preliminary works had studied on BC activated carbon using H_3PO_4 and KOH solution as activating agents and then carbonized at different temperature. It was shown that activated carbons obtained by acid activation had mesoporous structure with higher surface area (1,000 -2,500 m^2/g), whereas those from basic activation had more variance and larger porous structure with much less surface area (400-600 m^2/g).

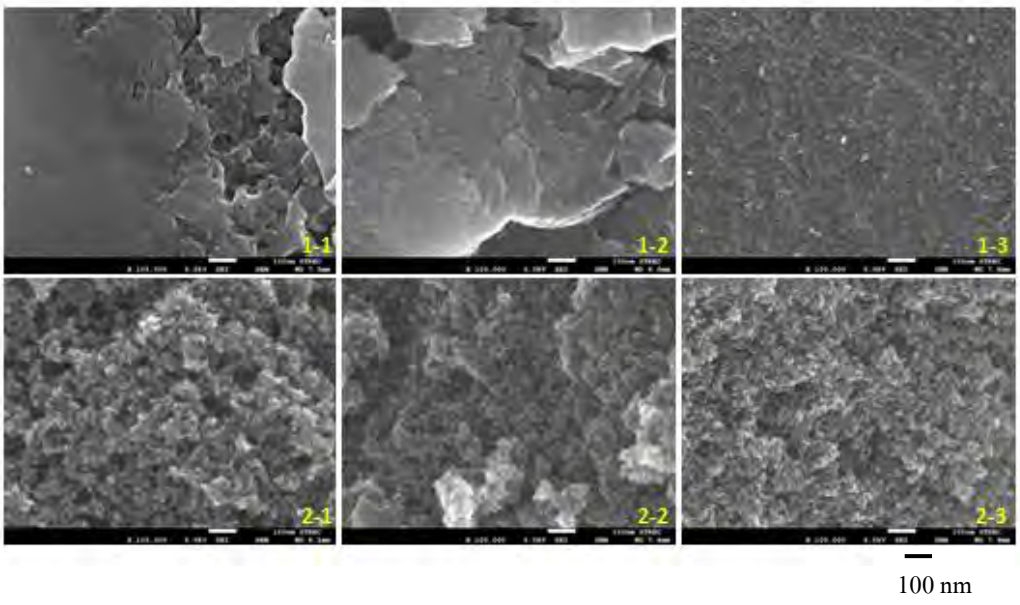

Figure 1. SEM images of BC activated carbons treated by H_3PO_4.

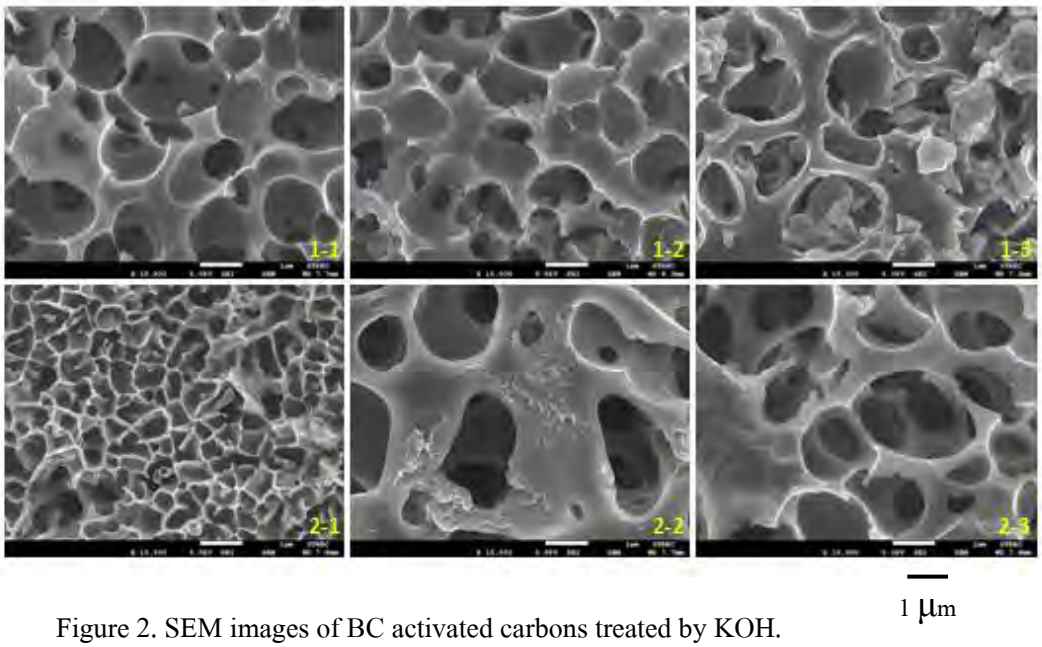

Figure 2. SEM images of BC activated carbons treated by KOH.

1.3.2 Ethanol dehydration

Ethanol dehydration reaction [10, 12] is a removal of water from alcohol to produce ethylene and acetaldehyde as the main products followed byproduct including di-ethyl ether. This reaction is an endothermic reaction which requires acid catalyst such as phosphoric acid and sulfuric acid and requires a lower temperature than hydrocarbon cracking, leading to an energy cost reduction that is more environmental friendly. Recently, different catalysts such as zeolite, alumina and silica–alumina have been investigated as solid catalyst for this process. The reaction temperature is 180-500^{o}C in gas phase. The chemical reactions are illustrated as below

C_2H_5OH ----> $C_2H_4 + H_2O$ +44.9 KJ/mol

C_2H_5OH ----> $CH_3CHO + H_2$ +52.3 kJ/mol

$2C_2H_5OH$ ----> $C_2H_5OC_2H_5 + H_2O$ -25.1 KJ/mol

1.3.3 Adsorption study

Adsorption technology [13] is a technique for removing micro pollutants from aqueous solutions such as organic and inorganic micro pollutants or colored and colorless organic pollutants. Adsorption process is considered as an important application for separation and purification in industrial processes using suitable adsorbents. The quality of adsorption depends on characteristics of the adsorbent including polarity, pore size and spacing. Adsorption experiments were conducted in liquid phase and the maximum adsorption capacity was determined. Experimental data were modeled using the Langmuir, Freundlich and Redlich–Peterson adsorption models to investigate the equilibrium isotherms, adsorption capacity and ability of the adsorbent to remove pollutants in aqueous solution.

2. Materials and Methods

2.1 Materials

Bacterial cellulose (BC) used in this project was supplied from the Institute of Research and Development of Food Product, Kasetsart University, Bangkok, Thailand. BC was synthesized by *A. xylinum* AGR 60. All the chemicals used in this project including sodium hydroxide (NaOH), potassium hydroxide (KOH), phosphoric acid (H_3PO_4), hydrochloric acid (HCl) and methylene blue (MB) were purchased from Sigma-Aldrich.

2.2 Methods

2.2.1 Bacterial cellulose preparation

BC hydrogel was treated with 1% w/v NaOH for 24 hours to remove bacterial cells, and then was rinsed with deionized (DI) water until pH was 7.0 and dried at 110°C for 24 hours.

2.2.2 Activated carbon preparation

BC was first activated via 85% H_3PO_4 with the ratio of 1:1 w/w and dried at 110^{o}C for 24 hours. Then, it was carbonized in the furnace at the temperature of 400-600^{o}C for 1 hour. The activated carbon (AC) was washed in stirred 1 molar HCl solution at 70^{o}C for 4 hours and then washed with DI water until the pH of 7 was reached. Then, the AC was dried at 110^{o}C for 24 hours.

2.2.3 *Characterization*

The morphology of the BC-AC was detected by scanning electron microscope (SEM). SEM model was JEOL mode JSM-5900LV from the Scientific and Technological Research Equipment Center, Chulalongkorn University (STREC). The pore diameter, pore volume, and surface area were determined via N_2 adsorption at liquid nitrogen temperature of -196^{o}C using a Micromeritics ASAP 2020 analyzer. The pore distribution, pore volume, and BET surface area were determined via the Brunauer-Emmett-Teller (BET) methods. Thermal gravimetric analysis (TGA) was performed at room temperature to 1000^{o}C at the heating rate of 10^{o}C per minute in N_2. The TGA's model was the SDT analyzer Model Q600 from TA instrument, USA. The functional groups of BC-ACs were detected via FT-IR analysis (Nicolet 6700 FTIR spectrometer).

2.2.4 Adsorption study

Methylene blue (MB) solution of 40 mL was prepared at concentration of 600 mg/L in 100 mL Erlenmeyer flasks. Then, 0.02 g of different BC-AC was added into methylene blue solution in each flask and incubated in an orbital shaker at 30^{o}C, 125 rpm for 6 hours. The samples were analyzed for MB concentration by UV-visible spectrophotometer (UV-2450; Shimadzu, Kyto, Japan) at the wavelength of 664 nm. The samples were collected to analyze at 5, 10, 20, 30, 40, 50, 60, 90, 120, 180, 240, 300, and 360 minutes.

2.2.5 Phosphoric acid catalyst preparation

The phosphoric acid was loaded into BC-ACs. Then, the loaded BC-ACs were dried in oven at 110°C for 20 hours before cooling down. After that, the BC-ACs were washed in deionized water until the pH of 7 was reached. Lastly, the obtained catalysts were dehydrated at 110^{o}C for 24 hours.

2.2.6 Catalytic activity examination

The catalytic activities of prepared BC-AC catalysts were examined via ethanol dehydration reaction at 200-400^{o}C with a temperature increment of 50^{o}C.

3. Results and discussions

3.1 Characterization

3.1.1 X-Ray Diffraction (XRD): The bulk crystal structure of BC-ACs was identified by using XRD technique (Figure 3); XRD patterns of activated carbon by various carbonization temperatures were investigated. According to XRD result, activated carbons derived from BC have only a diffraction peak around $2\theta = 22.50$, which can be describe as amorphous carbon composted of aromatic carbon sheets [14].

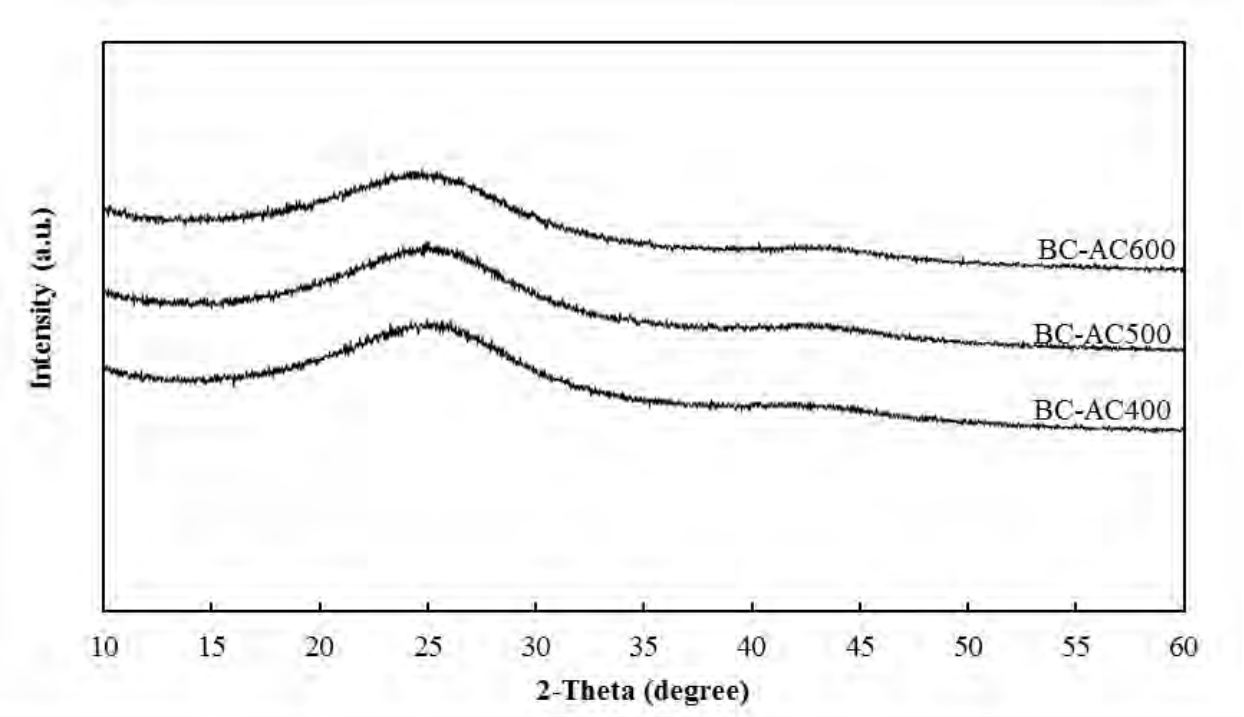

Figure 3. The XRD patterns of activated carbons derived from BC (BC-AC).

3.1.2 Chemical structure*:* The determination of functional group or chemical bonds existing in BC activated carbons (BC-AC) at various carbonization temperatures were measured in wave numbers by FT-IR spectra technique as shown in Figure 4. The broad band located around 3200-3700 cm^{-1} is attributed to the O-H stretching vibration of the hydroxyl group. It was formed from the adsorption of water vapor in surrounding and moisture residue during carbonization process. The band at 1600 and 1230 cm^{-1} are denoted as C=O and C-O stretching vibration of carbonyl groups, respectively due to the oxidative decomposition of organic species [15]. According to previous researchs [16-18], the broad bands are quite similar to activated carbons from difference biomass - based, which indicates the presence of the same functional groups. Other bands in the range of 1000-1200 cm^{-1} are the characteristic of phosphorous and

phosphor carbonaceous compounds from phosphoric acid activation. The band at 1100 cm^{-1} may be ascribed to the stretching vibration of hydrogen bonded P=O groups from phosphates or polyphosphates to O-C stretching vibrations in P-O-C (aromatic) linkage and to P=OOH [19]. The band that appears at 1000 cm-1 ascribe to ionized linkage P–O– in acid phosphate esters and symmetrical vibration in a P–O–P chain [20]. The bands at 885 and 830 are assigned to C-H stretching of aromatic compounds [21].

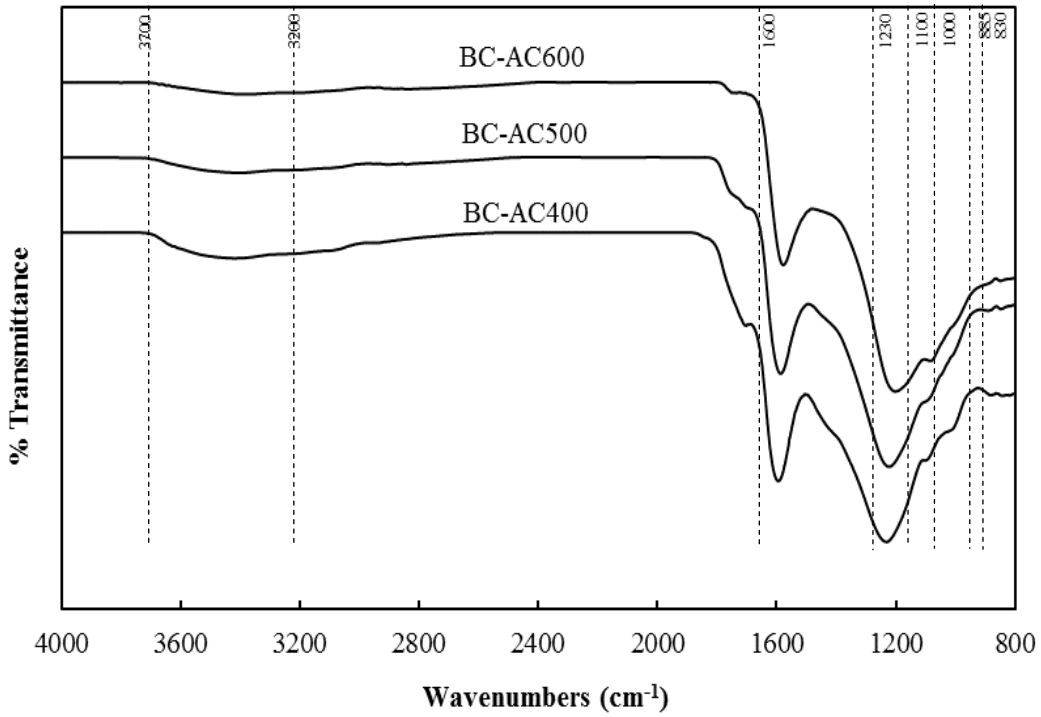

Figure 4 The FT-IR patterns of activated carbon derived from bacterial cellulose at various carbonization temperatures.

3.1.3 Porous structure: the structure of porosity; pore volume, pore size and specific surface area of activated carbon derived by BC (AC-BC) at various activation temperatures and drying method were determined by Nitrogen physisorption technique and compared to those of activated carbons derived from other biomaterials as shown in Table 1.

Table 1 Porous properties of activated carbons derived from BC (BC-AC) at various carbonization temperatures and the comparison to those of activated carbons derived from other biomaterials.

Material	Activating agent	S_{BET} (m^2/g)	V_t (cm^3/g)	D_p (nm)	Reference
BC-AC400	H_3PO_4	1,540	0.87	2.25	This work
BC-AC500	H_3PO_4	1,734	1.01	2.33	
BC-AC600	H_3PO_4	1,702	1.01	2.37	
Cotton stalk	H_3PO_4	1,720	0.89	-	22
Coconut shell	CO_2	1,700	1.14	2.70	23
Hazelnut bagasse	KOH	1,642	0.96	-	24
Bamboo	KOH	1,533	0.50	-	25
Deoiled rice bran residues	$ZnCl_2$	1,385	0.68	1.98	26
Deoiled rice bran residues	H_3PO_4	1,187	0.61	2.22	26
Mangosteen	K_2CO_3	1,123	0.56	1.98	27
Almond treepruning	Steam	1,080	0.95	-	28
Durian shell	H_3PO_4	1,024	0.35	2.50	29
Rice husk	$ZnCl_2$	927	0.56	0.80	30
Bagasse	$ZnCl_2$	923	0.53	0.80	30
Coir pith	$ZnCl_2$	910	0.36	1.60	31
Apricot stone	$ZnCl_2$	814	0.43	34.7	32
Olivestone	Steam	813	0.55	-	28
Wood apple outer shell	$ZnCl_2$	794	0.47	-	33
Walnutshell	Steam	792	0.52	-	28
Pistachio-nut shell	CO_2	778	0.47	-	34
Hazelnut shell	$ZnCl_2$	647	0.35	34.0	32
Cocoa podhusk	$K2CO_3$	615	0.31	2.0	35
Almond shell	Steam	601	0.37	-	28
Sugarcane bagasse	Steam	320	0.17	2.10	36
Peanut hull	Steam	253	0.22	-	37
Palm kernel shell	KOH	217	0.12	-	38
Acacia mangim wood	KOH	5.25	0.015	11.79	39

Where: S_{BET} = BET surface area; V_{total} = Total pore volume; D_p = Average pore diameter

***3.1.4. Surface morphology*:** the surface morphologies of BC-ACs were observed by SEM as shown in Figure 5. In the comparison to surface morphology of BC, the surface morphology of all BC-ACs after carbonization by H_3PO_4 activation was rougher, consisting of irregular small pores because of the evaporation of H_3PO_4 and other volatiles during the carbonization.

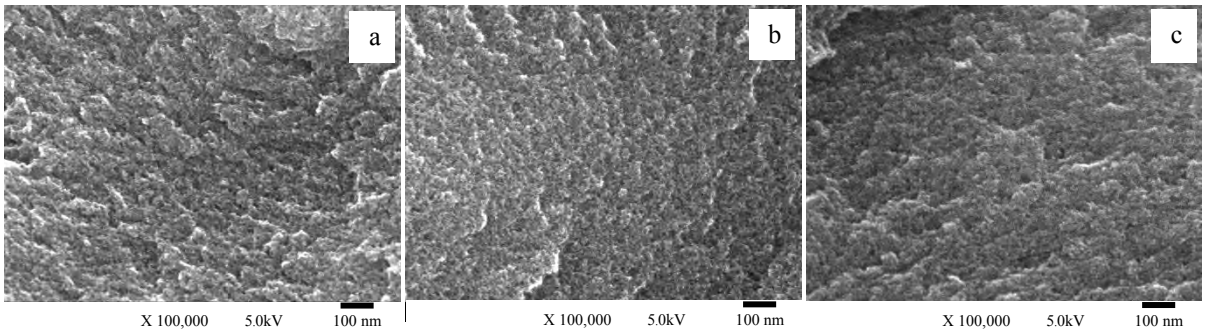

Figure 5. SEM micrographs of activated carbon derived from bacterial cellulose at various carbonization temperatures; BC-AC400 (a), BC-AC500 (b), and BC-AC600 (c).

3.1.5. Thermal stability: the mass loss during thermal gravimetric analysis of BC-AC at various carbonization temperatures is shown in Figure 6. The trends of TGA patterns of all BC-ACs are similar. The initial small mass loss at temperature around room temperature to 100°C could be attributed to moisture elimination. At 100 to 500°C, only small amount of carbon decomposition (less than 5 % of initial weight for BC-AC400 and BC-AC500; less than 2% of initial weight for BC-AC600) was detected, indicating that BC-ACs had high stability in the temperature range between 0 to 500°C.

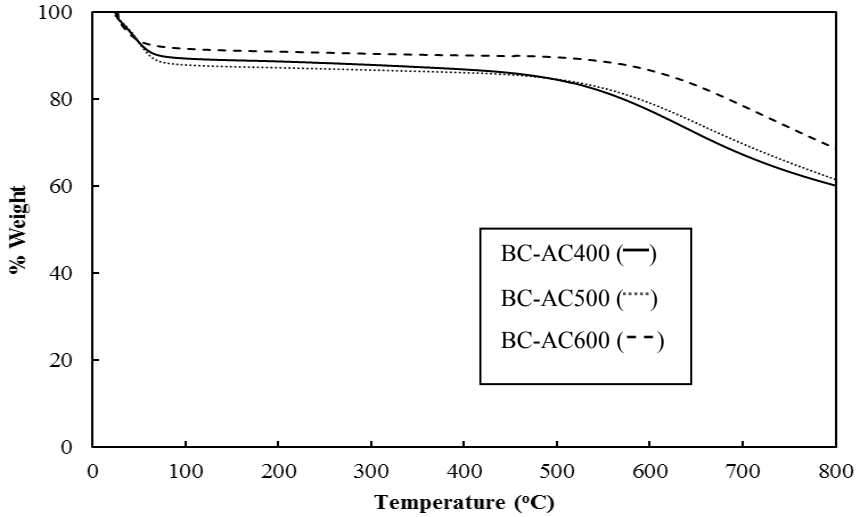

Figure 6.Thermal gravimetric of BC-ACs at various carbonization temperatures;

3.2 Development of novel catalyst of Al/BC (รายละเอียดเพิ่มเติมในภาคผนวก 1)

A novel catalyst of Al/BC was successfully developed by soaking purified bacterial cellulose (BC) hydrogel in aluminum nitrate aqueous solution, dehydration and calcination. Summarization of the procedure for the Al/BC preparation is shown in Figure 7. The Al/BC catalysts reveal interior meso–macro porous structures with average pore diameters in the range of 17–34 nm. The Al/BC catalyst has many promising properties, such as good metal dispersion, high chemical and thermal stabilities. The high yield of diethyl ether at ~ 42 % can be produced from ethanol at 200 °C with the selectivity of almost 100% by using Al/BC as catalyst in ethanol dehydration. The comparison of catalytic activity of Al/BC with others in ethanol dehydration is shown in Table 2.

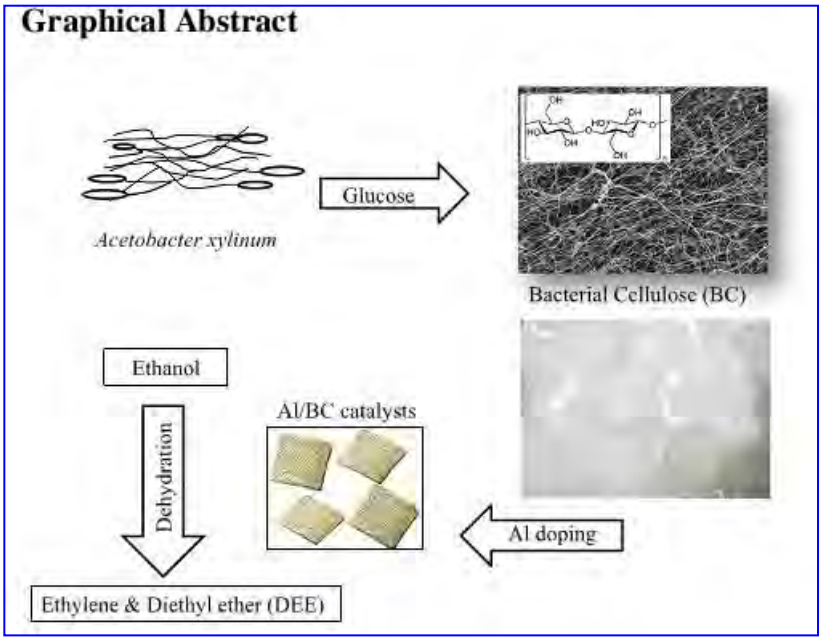

Figure 7. Summarization of the procedure for the Al/BC preparation [14.].

Table 2 Catalytic activity of Al/BC catalyst as compared to other catalysts [14]

Catalysts	Surface area (m^2/g)	Pore diameter (nm)	Reaction temperature (°C)	Ethanol conversion (%)	Ethylene yield (%)	DEE yield (%)
25Al/BC-TD	18	25.6	200–400	41.5–54.6	0.0–35.4	41.6–13.4
25Al/BC-FD	22	26.3	200–400	41.3–65.7	1.1–43.3	40.0–17.6
Al-com	137	3.9	200–400	0–95	0.0–71.3	0.0–0.0
Al-SG	152	3.5	200–400	15–98	6.8–78.4	7.0–0.0
Al-SV	215	9.3	200–400	10–100	2.5–100	7.5–0.0
Al-SSP	443.6	5.9	200–400	20–85	18.6–82.0	1.4–0.0
HBZ	522	2.2	200–400	7–100	0.0–99.4	7.1–0.0
Al-HBZ	306	3.4	200–400	9–92	0.0–90.2	9.5–1.8
M-Al	195	9.0	200–400	12–92	0.0–88.9	12.5–2.5

3.3 Adsorption study (รายละเอียดเพิ่มเติมในภาคผนวก 2 และ 3)

BC-AC600 and BC-AC500 had very high adsorption capacity with the maximum MB absorption of 507.5 and 504.4 mg/g, respectively, whereas BC-AC400 had relatively less adsorption capacity of 393.0 mg/g. The increasing of the surface area could encourage improved adsorption capacity due to more interaction between active sites of adsorbents and molecules of MB [40]. Considering the removal of MB, the percent removal of MB increased with the increase of the contact time, until the equilibrium was reached (Figure 8). The removal of MB of all BC-ACs at 100% could be achieved if the initial MB concentration was not greater than 100 mg/L. This is because the ratio of active site and MB molecule at low concentration is high, therefore all MB molecules could be adsorbed on active sites of the adsorbents [41]. BC-AC400, BC-AC500 and BC-AC600 showed the MB removal at 88.4, 99.8, and 99.8%, respectively, when the initial MB concentration was 200 mg/L. The removal of MB relatively decreased with the increase of the initial MB concentration from 200 to 600 mg/L. The results indicated that BC-ACs are effective absorbents for the removal of MB from the solution, especially for the solutions with MB concentration $\leq$ 200 mg/L.

Table 3 The maximum adsorption capacity for MB removal by BC-ACs as compared to those by ACs derived from other cellulosic materials.

Adsorbent	q_m (mg/g)	Reference
BC-AC400	393.0	This work
BC-AC500	505.8	This work
BC-AC600	507.5	This work
Coconut husk-based AC	434.8	[42]
Peach stones-based AC	412.0	[43]
Date stone-based AC	398.2	[44]
Oil palm shell-based AC	303.0	[45]
Coconut shell-based AC	277.9	[46]
Oil palm fiber-based AC	277.8	[46]
Ground shell-based AC	164.9	[47]
Bamboo dust-based AC	143.2	[47]
Activated sewage char	120.0	[48]
Rice husk-based AC	60.1	[49]

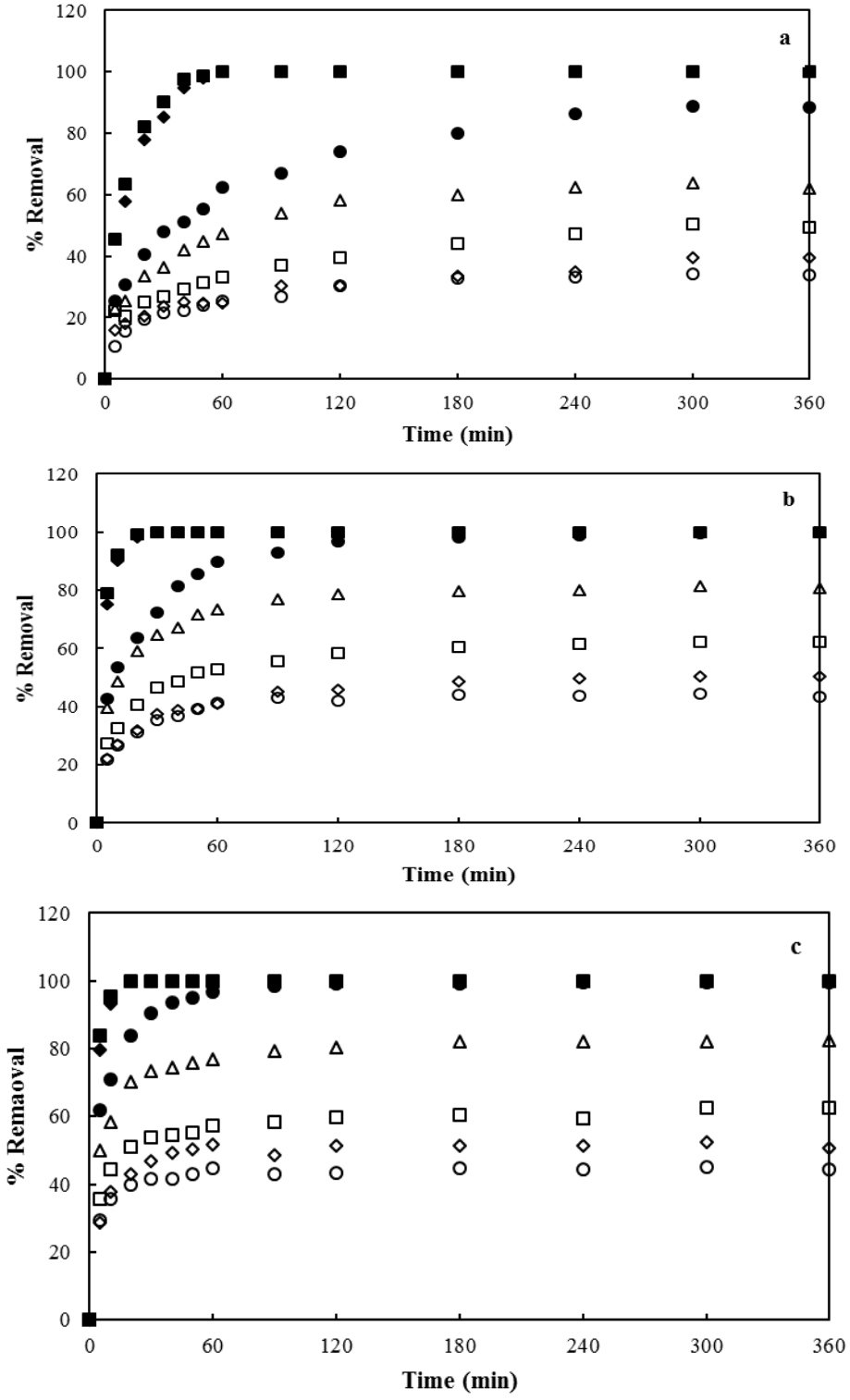

Figure 8 Removal of MB at difference initial MB concentration (■50, ♦100, ●200, △300, □400, ◊500, and ○600 mg/L) on difference BC-ACs; BC-AC400 (a), BC-AC500 (b), and BC-AC600 (c).

4. Conclusion

The production of high surface area activated carbon from biomass has attracted attentions due to its wide range of applications. In this research, bacterial cellulose (BC) is used as carbon source for activated carbon preparation due to its highly nanoporous structure and eco-friendliness. BC was carbonized with a chemical activation process using phosphoric acid (H_3PO_4) as an activating agent at different temperatures (400, 500 and 600 °C). The carbonization temperature significantly affected the porous structure of BC-AC. The carbonization temperature at 500°C exhibits the highest surface area of 1,734.2 m^2/g with the total pore volume of 1.011 cm^3/g. BC-ACs had mesoporous structure with the average pore diameter of 2.2-2.4 nm. BC-ACs had high stability in the temperature between 100 to 500°C.

By using BC-AC500 or BC-AC600 for MB removal, the equilibrium could be reached within 10 min for the system with low MB concentration (50-100 mg/L) and 240 min with high MB concentration (200-600 mg/L). The removal of MB from the solution with the initial MB concentration not greater than 200 mg/L was almost 100%. From the experimental study, the maximum MB adsorption capacity of BC-AC400, BC-AC500, and BC-AC600 were 393.0, 505.8, and 507.5 mg/g, respectively, which were very close to the values of maximum adsorption capacity (q_m) estimated from Langmuir model. The Redlich-Peterson was shown to be the best-fitting model with R^2 value of 1.000 for all BC-ACs. BC-AC was found very effective for using as an adsorbent to remove MB from water.

Besides, BC and BC activated carbon has been further developed as catalyst supports. A novel catalyst of Al/BC was developed by soaking purified BC hydrogel in aluminum nitrate aqueous solution, dehydration and calcination. The Al/BC catalyst has many promising properties as catalyst in ethanol dehydration, such as good metal dispersion, high chemical and thermal stabilities. The high yield of diethyl ether at ~ 42 % can be produced from ethanol at 200 °C with the selectivity of almost 100% by using Al/BC as catalyst in ethanol dehydration.

In the future, we plan to continue developing BC-AC catalysts for the ethanol dehydration reaction. Modification of the porous structure for improved mass transfer rate and enhanced product selectivity will be carried out. Experimental studies will be performed in order to develop a simple and effective method for producing effective solid catalysts from BC-AC as an alternative eco-friendly catalyst.

References

[1] Adib Yahya, Mohd; Al-Qodah, Z.; and Zanariah Ngah, C.W. Agricultural bio-waste materials as potential sustainable precursors used for activated carbon production: A review. Renewable and Sustainable Energy Reviews 46 (2015): 218–235

[2] Siriwardane, V. R.; Shen S. M.; Fisher P. E.; and Poston, A. J. Adsorption of CO2 on Molecular Sieves and Activated Carbon. Energy Fuels 15 2(2001): 279-284.

[3] Wu, X.; Zhu, F.; Qi, J.; and Zhao, L. Biodiesel production from sewage sludge by using alkali catalyst catalyze. Procedia Environmental Sciences 31 (2016): 26–30.

[4] Kadirvelu, K.; Thamaraiselvi, K.; and Namasivayam, C. Removal of heavy metals from industrial wastewaters by adsorption onto activated carbon prepared from an agricultural solid waste. Bioresource Technology 761 (2001): 63-65.

[5] Sircar, S.; Golden, C. T.; Rao, B. M. Activated carbon for gas separation and storage. Carbon 34, (1996): 1-12.

[6] Altenor, S.; Carene, B.; Emmanuel, E.; Lambert, J.; Ehrhardt, JJ.; and Gaspard, S. Adsorption studies of methylene blue and phenol onto vetiver roots activated carbon prepared by chemical activation. J Hazard Mater 169 (2009): 1029–1039.

[7] Orkun, Y.; Karatepe, N.; and Yavuz, R. Influence of temperature and impregnation ratio of H3PO4 on the production of activated carbon from hazelnut shell. Acta Phys Pol A 121 (2012): 277–280.

[8] Olafadehan, OA.; Jinadu, OW.; Salami, L.; and Popoola, OT. Treatment of brewery waste water effluent using activated carbon prepared from coconut shell. Int J Appl Sci Technol 2 (2012): 165–178.

[9] Kirdponpattara, S. Properties and application of bacterial cellulose-alginate composite sponges. Doctoral's Thesis, Department of Chemical Engineering, Faculty of Engineering, Chulalongkorn University, 2012.

[10] Phanthang, L. Characteristics of activated carbon derived from bacterial cellulose and its application as a catalyst support. Master's Thesis, Department of Chemical Engineering, Faculty of Engineering,Chulalongkorn University, 2013.

[11] Boongate, C.; and Phisalaphong, M. Activated carbons from bacterial cellulose by chemical activation with potassium hydroxide. International conference on science and technology, Bangkok: RMUTT, 2015.

[12] Chatchawanrat, S. Dehydrogenation of ethanol to acetaldehyde over activated carbon catalyst. Master's Thesis, Department of Chemical Engineering, Faculty of Engineering, Chulalongkorn University, 2013.

[13] Emad N. El Qada; Allen, J. S.; and Walker, M. G. Adsorption of Methylene Blue onto activated carbon produced from steam activated bituminous coal: A study of equilibrium adsorption isotherm. Chemical Engineering Journal 124 (2006): 103–110.

[14] Ibnu Abdulwahab, M.; Khamkeaw, A.; Jongsomjit, B.; and Phisalaphong, M. Bacterial Cellulose Supported Alumina Catalyst for Ethanol Dehydration. Catalysis Letters 147(2017): 2462-2472.

[15] Finocchio, E.; Cristiani, C.; Dotelli, G.; Stampino, P.G.; Zampori, L. Thermal evolution of PEG-based and BRIJ-based hybrid organo-inorganic materials. FT-IR studies, Vib. Spectrosc. 71 (2014): 47-56.

[16] Chen, Y.; Huang, B.; Huang, M.; Cai, B. On the preparation and characterization of activated carbon from mangosteen shell, J.Taiwan Inst. Chem. E. 42 (2011): 837-842.

[17] Oliveira, L.C.A.; Pereira, E.; Guimaraes, I.R.; Vallone, A.; Pereira, M.; Mesquita, J.P.; Sapag, K. Preparation of activated carbons from coffee husks utilizing $FeCl_3$ and $ZnCl_2$ as activating agents, J. Hazard. Mater. 165 (2009): 87-94.

[18] Shi, Q.; Zhang, J.; Zhang, C.; Li, C.; Zhang, B.; Hu, W.; Xu, J.; Zhao, R. Preparation of activated carbon from cattail and its application for dyes removal, J.Environ. Sci. 22 (2010): 91-97.

[19] Yorgun, S.; Yıldız, D. Preparation and characterization of activated carbons from Paulownia wood by chemical activation with H_3PO_4, J. Taiwan Inst. Chem. E. 53 (2015): 122-131.

[20] Yakout, S.M.; Sharaf El-Deen, G. Characterization of activated carbon prepared by phosphoric acid activation of olive stones, Arab. J. Chem. 9 (2016): S1155-S1162.

[21] Pereira, R.G.; Veloso, C.M.; Silva, N.M.; Sousa, L.F.; Bonomo, R.C.F.; Souza, A.O.; Souza, M.O; Fontan, R. Preparation of activated carbons from cocoa shells and siriguela seeds using H_3PO_4 and $ZnCl_2$ as activating agents for BSA and α-lactalbumin adsorption, Fuel Process.Technol. 126 (2014): 476-486.

[22] Nahil, MA., et al., Pore characteristics of activated carbons from the phosphoric acid chemical activation of cottons talks. Biomass Bioenergy 37 (2012): 142–9.

[23]Guo, S., et al., Effects of CO_2 activation on porous structures of coconut shell-based activated carbons. Appl Surf Sci, 255 (2009): 8443–8449.

[24] Demiral, H., et al., Pore structure of activated carbon prepared from hazelnut bagasse by chemical activation. Surf Interface Anal 40 (2008): 616–619.

[25] Hirunpraditkoon, S., et al., Adsorption capacities of activated carbons prepared from bamboo by KOH activation. World Acad Sci Eng Technol, 78 (2011): 711–715.

[26]Niticharoenwong, B., et al., Characteristics of activated carbons derived from deoiled rice bran residues. Chemical Engineering Communications, 200 (2013): 1309-1321.

[27] Chen, Y., et al., On the preparation and characterization of activated carbon from mangosteen shell. Journal of the Taiwan Institute of Chemical Engineers, 42(2011): 837-842.

[28] Gonzalez, J.F., et al., Pyrolysis of various biomass residues and char utilization for the production of activated carbons. J Anal Appl Pyrol, 85(2009): 134–141.

[29] Jun, T.Y., et al., Effect of activation temperature and heating duration on physical characteristics of activated carbon prepared from agriculture waste. Environ Asia, 3 (2010): 143–148.

[30] Boonpoke, A., et al., Synthesis of activated carbon and MCM-41 from bagasse and rice husk and their carbon dioxide adsorption capacity. J Sustain Energy Environ, 2(2011): 77–81.

[31] Subha, R., et al., Zinc chloride activated coir pith carbon as low cost adsorbent for removal of 2,4-dichlorophenol: equilibrium and kinetics tu- dies. Indian J Chem Technol, 14(2009): 471–479.

[32] Ozcimen, D., et al., Adsorptionofcopper(II)ions on to hazelnut shell and apricot stone activated carbons. Adsorp Sci Technol, 28(2010): 327–41.

[33] Bhadusha, N., et al., Adsorptive removal of methylene blue onto ZnCl2 activated carbon from wood apple outer shell: kinetics and equilibrium studies. E-JChem, 8(2011): 1696–1707.

[34] Lua, A.C., et al., Effect of pyrolysis conditions on the properties of activated carbon prepared from pistachio-nutshells. J Anal Appl Pyrol, 72 (2004): 279–287.

[35] Cruz, G., et al., Production of activated carbon from Cocoa (Theobroma cacao) pod husk. Civ Environ Eng, 2(2012): 1–6.

[36] Devnarain, P.B., et al., Production of activated carbon from South African sugar cane bagasse. Proc SAfr Sug Tech Ass, 76(2002): 477–489.

[37] Girgis, B.S., et al., Characteristics of activated carbon from peanut hulls in relation to conditions of preparation. Mater Lett, 57 (2002): 164–172.

[38] Abechi, S.E., et al., Preparation and characterization of activated carbon from Palm Kernel shell by chemical activation. Res J Chem Sci, 3(2013): 54–61.

[39] Danish, M., et al., Characterization of Acacia mangium wood based activated carbons prepared in the presence of basic activating agents. Bioresources, 6(2011): 3019–3033.

[40] Aguayo-Villarreal, I.A.; Bonilla-Petriciolet, A.; Muñiz-Valencia, R. Preparation of activated carbons from pecan nutshell and their application in the antagonistic adsorption of heavy metal ions, J. Mol. Liq. 230 (2017): 686-695.

[41] Geçgel, Ü.; Özcan, G.; Gürpınar, G.Ç. Removal of methylene blue from aqueous solution by activated carbon prepared from pea shells (Pisum sativum), J. Chem-Ny. 2013 (2013): 9.

[42] Tan, I.A.W.; Ahmad, A.L.; Hameed, B.H. Adsorption of basic dye on high-surface-area activated carbon prepared from coconut husk: Equilibrium, kinetic and thermodynamic studies, J. Hazard. Mater. 154 (2008): 337-346.

[43] Attia, A.A.; Girgis, B.S.; Fathy, N.A. Removal of methylene blue by carbons derived from peach stones by H_3PO_4 activation: Batch and column studies, Dyes Pigments 76 (2008): 282-289.

[44] Ahmed, M.J.; Dhedan, S.K. Equilibrium isotherms and kinetics modeling of methylene blue adsorption on agricultural wastes-based activated carbons, Fluid Phase Equilibr. 317 (2012): 9-14.

[45] Tan, I.A.W.; Ahmad, A.L.; Hameed, B.H. Enhancement of basic dye adsorption uptake from aqueous solutions using chemically modified oil palm shell activated carbon, Colloid. Surface A. 318 (2008): 88-96.

[46] Tan, I.A.W.; Hameed, B.H.; Ahmad, A.L. Equilibrium and kinetic studies on basic dye adsorption by oil palm fibre activated carbon, Chem. Eng. J. 127 (2007): 111-119.

[47] Kannan, N.; Sundaram, M.M. Kinetics and mechanism of removal of methylene blue by adsorption on various carbons—a comparative study, Dyes Pigment 51 (2001): 25-40.

[48] Sainz-Diaz, C.I.; Griffiths, A.J. Activated carbon from solid wastes using a pilot-scale batch flaming pyrolyser, Fuel 79 (2000): 1863-1871.

[49] El-Halwany, M.M. Study of adsorption isotherms and kinetic models for Methylene Blue adsorption on activated carbon developed from Egyptian rice hull (Part II), Desalination 250 (2010): 208-213.

5. Output of the research (international journal publication / international conference)

5.1 Bacterial Cellulose Supported Alumina Catalyst for Ethanol Dehydration,
International journal publication (IF in 2016= 2.799), Catalysis Letters: 147:2462–2472, 2017
(Appendix 1)

5.2 Characteristics of Activated Carbon Derived from Bacterial Cellulose and Its Application as an Adsorbent, Oral presentation in the 3th Symposium on Bacterial NanoCellulose, Fukuoka, Japan (16-17 Oct, 2017) (Appendix 2)

5.3 Activated Carbon from Bacterial Cellulose as an Effective Adsorbent for Removing Dye from Aqueous Solution, International journal publication (IF in 2016= 1.106), Separation Science and Technology (submitted) (Appendix 3)

ภาคผนวก(Appendix) 1

Catal Lett (2017) 147:2462–2472
DOI 10.1007/s10562-017-2145-y

Bacterial Cellulose Supported Alumina Catalyst for Ethanol Dehydration

M. Ibnu Abdulwahab[1,2] · A. Khamkeaw[1,2] · B. Jongsomjit[2] · M. Phisalaphong[1]

Received: 28 March 2017 / Accepted: 9 July 2017 / Published online: 20 July 2017

Abstract An ultrafine three-dimensional nanofiber network structure of a very high porosity endows bacterial cellulose (BC) to function as support for heterogeneous catalysis. A novel catalyst of BC supported alumina (Al_2O_3) was developed by soaking purified BC hydrogel in aluminum nitrate ($Al(NO_3)_3$) aqueous solution, dehydration (hot air drying and freeze-drying) and calcination. The Al/BC catalysts reveal interior meso–macro porous structures with average pore diameters in the range of 17–34 nm. The catalytic activities were examined through an ethanol dehydration reaction in the gas phase at atmospheric pressure in the range of 200–400 °C. The effects of acidic metal loading and dehydration methods were investigated. Increasing Al loading from 12 to 50% resulted in a decreased surface area but an increase in pore size. At the same Al loading, the catalysts with a dehydration process by hot air drying presented higher Al concentrations on the outer surface compared with those by freeze-drying. At high temperature of 400 °C, Al/BC catalysts with 25 wt% Al loading and dehydrated by freeze drying (25Al/BC FD) and 50 wt% Al loading, dehydrated by hot air drying (50Al/BC TD) exhibited the highest ethanol conversions of 65.7–66.4% and ethylene yields of 43.26–44.24%, respectively, whereas at low temperature of 200 °C, Al/BC catalysts with 25 wt% Al loading with either dehydration method exhibited the highest diethyl ether yields of 40.02–41.60%.

Graphical Abstract

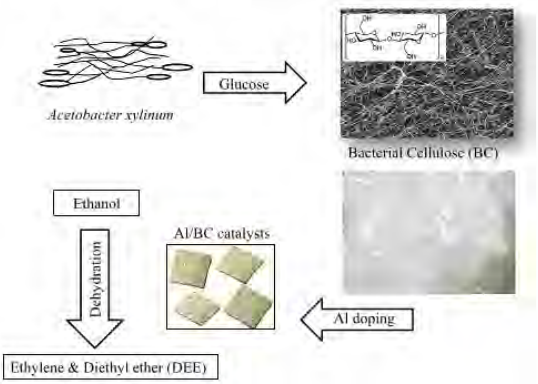

Keywords Catalyst support · Composites · Reaction · Bacterial cellulose · Alumina · Ethanol dehydration

1 Introduction

Carbon materials show several advantages as supports in heterogeneous catalysis, including highly porous structure, high stabilities at high temperatures in non-oxidizing atmospheres, renewable resources, low-cost and environmental friendly materials [1–4]. Cellulose is the most abundant carbon source, mainly obtained from plant-based materials. Very few species of bacteria can also produce cellulose. Plant-based cellulose generally contains impurities such as lignin and hemicellulose, whereas bacterial cellulose (BC) is nearly pure cellulose [5]. BC can be

✉ M. Phisalaphong
Muenduen.p@chula.ac.th

[1] Chemical Engineering Research Unit for Value Adding of Bioresources, Department of Chemical Engineering, Faculty of Engineering, Chulalongkorn University, Bangkok 10330, Thailand

[2] Center of Excellence on Catalysis and Catalytic Reaction Engineering, Department of Chemical Engineering, Faculty of Engineering, Chulalongkorn University, Bangkok 10330, Thailand

extracellularly synthesized into nanosized fibrils by the bacteria *Acetobacter xylinum*, and glucose is used as a common substrate. Plant-derived cellulose and BC have the same chemical structure; however, BC displays superior physical and chemical properties to plant-derived cellulose, including ultrafine nanofiber network structure, extensive surface area, high mechanical strength, high crystallinity, high chemical stability and high hydrophilicity [5, 6]. Those advantageous properties could endow BC to function as excellent matrix or support for heterogeneous catalysis. Recently, CdS nanoparticles/BC hybrid nanofibers was successful developed for photocatalysis application by deposition of CdS nanoparticles onto the substrate of hydrated BC nanofibers (BCF) [7]. However, up till now, there has been very little information available on the utilization of BC for the application as catalyst supports.

Ethanol production from renewable carbohydrate materials has attracted worldwide interest in its use as a carbon source for chemical and fuel production. Ethylene and diethyl ether (DEE) are the main products of ethanol dehydration reaction. Ethylene can be used as a polymerization raw material to produce a variety of important organic chemical products such as polyethylene, polyvinyl chloride, and polystyrene. Ethylene is also used as the precursor for synthesizing ethylene oxide, ethylene dichloride, ethylene glycol, and ethylbenzene [8–11]. DEE is widely used as a solvent for waxes, fats, oils, perfumes, alkaloids, and gums. DEE is also used as a fuel additive for biodiesel or diesel fuels to improve engine performance and emission properties. Dehydration of ethanol over solid acid catalysts to produce ethylene and DEE requires a lower temperature than hydrocarbon cracking, leading to an energy cost reduction that is more ecofriendly. Recently, different catalysts such as zeolite [12, 13], alumina [14, 15], silica [16], and silica–alumina [17] have been investigated to increase ethanol conversion and lower reaction temperature [9]. Among them, alumina is an efficient catalyst because of its excellent thermal stability and lower acid strength [18–20]. Moreover, alumina is cheap and readily available; it is suitable for industrial applications. However, the reaction temperature for the use of pure alumina or modified alumina catalysts is relatively high (usually more than 350 °C), thus the production consumes high amount of energy [9, 11]. By using zeolite catalysts, the operating temperature could be reduced; however its stability is poor and easily deactivated through carbon deposition [11]. In addition, the porous structure of those catalysts should be improved to prevent internal mass transport limitation.

BC displays excellent physical and chemical properties, such as ultrafine nanofiber network structure, high porosity and high mechanical strength. Therefore, in order to modify the pore structure of alumina catalyst, aluminum was loaded into a BC nanofiber and its application was explored for the catalysis of ethanol dehydration to ethylene and diethyl ether (DEE). Important factors that influence the reaction rate and selectivity including temperature, acidity, and porous structure of the catalysts were investigated [18, 21]. The influences of acidic metal loading and dehydration methods are examined to optimize the catalyst preparation method for ethanol dehydration.

2 Materials and Methods

2.1 Materials

BC was synthesized by *A. xylinum* AGR 60. The stock culture was kindly provided by Pramote Thammarad, The Institute of Research and Development of Food Product, Kasetsart University, Bangkok, Thailand. BC hydrogel was treated with 1% w/v NaOH to remove bacterial cells and was neutralized with 1% w/v acetic acid. The cleaned BC was rinsed with deionized water until pH was 7.0.

2.2 BC-Supported Alumina Catalyst Preparation

The purified wet BC hydrogel ($\approx 1 \times 1 \times 1$ cm^3) of 200 g was soaked in 200 ml $Al(NO_3)_3$ aqueous solution of various concentrations of 3, 7, and 14%w/v, producing approximately 12, 25, and 50 wt% Al after drying, respectively. The mixtures were stirred continuously for 12 h at room temperature to fully distribute Al into the BC matrix. The obtained BC/Al products were separated into two groups. One was dehydrated by hot air drying at 110 °C for 24 h and calcined in air at 200 °C for 4 h. The other one was freeze-dried under vacuum pressure (≈100 mTorr) for 24 h, dehydrated at 110 °C for 12 h and calcined in air at 200 °C for 4 h. All of the prepared catalysts were stored in plastic films at room temperature.

2.3 Catalyst Characterization

The surface area, pore volume, and pore diameter of catalysts were determined by nitrogen gas adsorption at liquid nitrogen temperature (−196 °C) using Micromeritics Chemisorb 2750 Pulse instrument (Norcross, GA, USA). Before characterization, the sample was thermally treated at 150 °C for 1 h.

XRD patterns of the catalysts were determined by Siemens D5000 X-ray diffractometer (Aubrey, TX, USA) using CuK_α radiation with a Ni filter in the 2θ range of 10°–80° with a resolution of 0.04°.

Scanning electron microscopy (JEOL JSM-5800LV, Tokyo, Japan) and energy dispersive X-ray spectroscopy were used to determine the surface morphology and elemental distribution of the catalyst particles. The energy dispersive X-ray spectroscopy was performed using a Link Isis Series 300

program at the Scientific and Technological Research Equipment Center, Chulalongkorn University, Bangkok, Thailand. Before analyzing the morphology, the samples were sputtered with platinum and photographed. The coated specimens were kept in a dry place before examination.

The functional groups of catalyst chemical structure were determined by Fourier transform infrared analysis using a Nicolet 6700 FTIR spectrometer (Thermo Scientific, Waltham, MA, USA).

The total acidic proton (H^+) upon the dissolution of the catalysts was determined using standard acid–base back titration. Approximately 0.1 g of catalyst sample was placed in an 250 ml-Erlenmeyer flask containing 60 ml of 0.008 M NaOH, and stirred at room temperature for 1 h. The excessive amount of NaOH was neutralized using 0.02 M HCl as the titrant.

The acid properties of catalysts were investigated by temperature-programmed desorption of ammonia (NH_3-TPD) using Micromeritics Chemisorb 2750 pulse chemisorption system. NH_3-TPD tests of the catalyst samples (0.2 g) were carried out under a helium gas flow of 30 cm/min. After chemisorption step, a helium gas was flown over catalyst to remove any adsorbed molecules from catalyst active site from temperature of 40–500 °C, at heating rate 10°/min. The spectrum of NH_3-TPD was deconvoluted by using a peak-fitting program, Fityk.

2.4 Catalytic Performance

Ethanol dehydration was performed in a glass fixed-bed continuous flow reactor with an inner diameter and length of 0.7 and 33 cm, respectively [18, 21]. The reactor was placed into a temperature-programmed tubular furnace. In each experiment, 0.01 g of a packed quartz wool and 0.05 g of catalyst were packed in the reactor, and the catalyst was then pretreated in argon (50 ml/min) at 200 °C for 1 h under atmospheric pressure. A feed consisting of 99.95% ethanol was fed into the reactor, and the reaction was performed under the controlled temperatures of 200, 250, 300, 350 and 400 °C, at atmospheric pressure. The effluent products were collected and analyzed by a Shimadzu GC8A gas chromatograph with a flame ionization detector using a capillary column (DB-5) at 150 °C.

$$\textit{Ethanol conversion}\ (\%) = \frac{(\textit{moles of ethanol in feed} - \textit{moles of ethanol in product}) \times 100}{\textit{moles of ethanol in feed}}$$

$$\textit{Selectivity}\ (\%) = \frac{\textit{moles of desired product formed} \times 100}{\textit{moles of total products formed}}$$

$$\textit{Yield}\ (\%) = \frac{\textit{selectivity} \times \textit{ethanol conversion}}{100}$$

3 Results and Discussion

3.1 Catalyst Characterization

3.1.1 Surface Morphology and Al Distribution

The purified wet BC hydrogel was soaked in aluminum nitrate ($Al(NO_3)_3$) aqueous solution producing approximately 12, 25, and 50 wt% of Al loadings after drying. The BC/Al products were dehydrated by hot air drying or freeze-drying. The sample names are xAl/BC-TD, where x is the wt% of Al loading after drying; i.e., 50Al/BC-TD refers to a BC-supported alumina catalyst with a 50 wt% Al loading (after drying), dehydrated by hot air drying. In a similar way, 50Al/BC-FD refers to a BC-supported alumina catalyst with a 50 wt% Al loading, dehydrated by freeze-drying.

Scanning electron microscopy images in Fig. 1 illustrate the surface morphologies of dried BC, Al/BC-TD, and Al/BC-FD catalysts. The catalyst particles showed an average width of 10–30 μm with a thickness of ≈10 μm. A rough surface with small clusters of Al particles on the surface was observed for the Al/BC catalysts. Higher-magnification views of surface morphology and cross section of the sample of Al/BC catalyst were shown in Fig. 2, in which the networks of carbon fibers on the catalyst surface and interior meso–macro porous structure were observed. It was shown that the average pore size of the Al/BC catalyst dehydrated by freeze-drying was relatively higher than that of the catalyst dehydrated hot air-drying Energy dispersive X-ray spectroscopy was used to map the elemental distribution and percentage on the support surface. The maps for Al distribution of catalysts dehydrated by hot air drying and freeze-drying are shown in Fig. 3. All of the Al/BC catalysts exhibited a good dispersion of Al on the surface of BC supports. As shown in Table 1, Al percentages on the surface of Al/BC catalysts increased with the loading content of Al. At the same loading contents of Al, Al/BC-TD presented a higher concentration of Al on the surface than those of the Al/BC-FD catalysts. During the dehydration by hot air drying, the high shrinkage in carbon structure created a more dense structure with less porosity, resulting in a higher percentage of alumina on the surface. Dehydration via freeze-drying produced catalysts with a significantly higher porosity than Al/BC-TD catalysts.

3.1.2 Acidity

Standard acid–base back titrations were used to examine the total acidic proton (H^+) upon the dissolution of the catalysts, and the result are shown in Table 1. The total H^+ of Al/BC catalysts were in the order: 50Al/

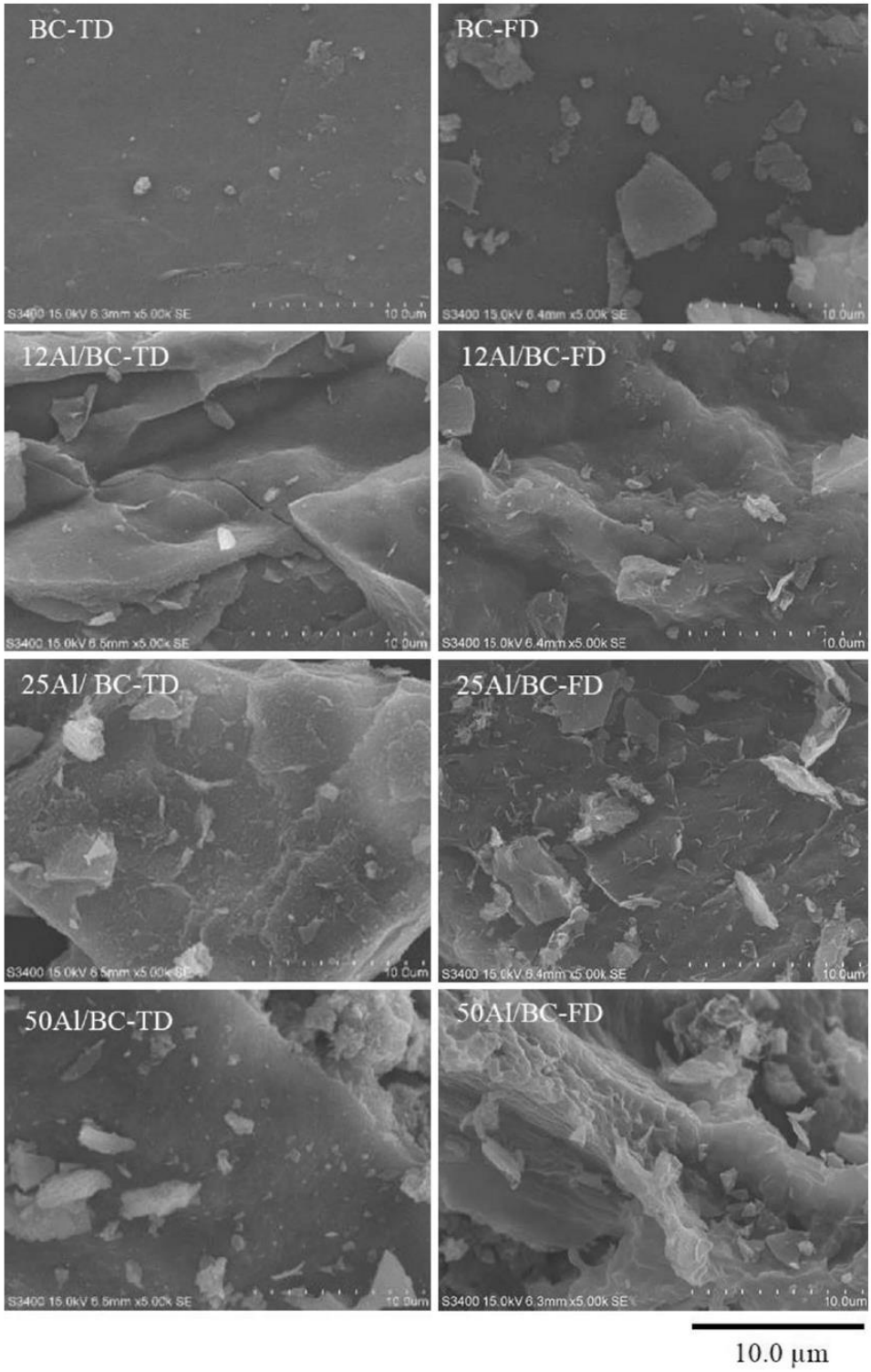

Fig. 1 SEM micrograph of surface morphology of BC and Al/BC catalysts dehydrated by hot air-drying (*left*) and by freeze-drying (*right*)

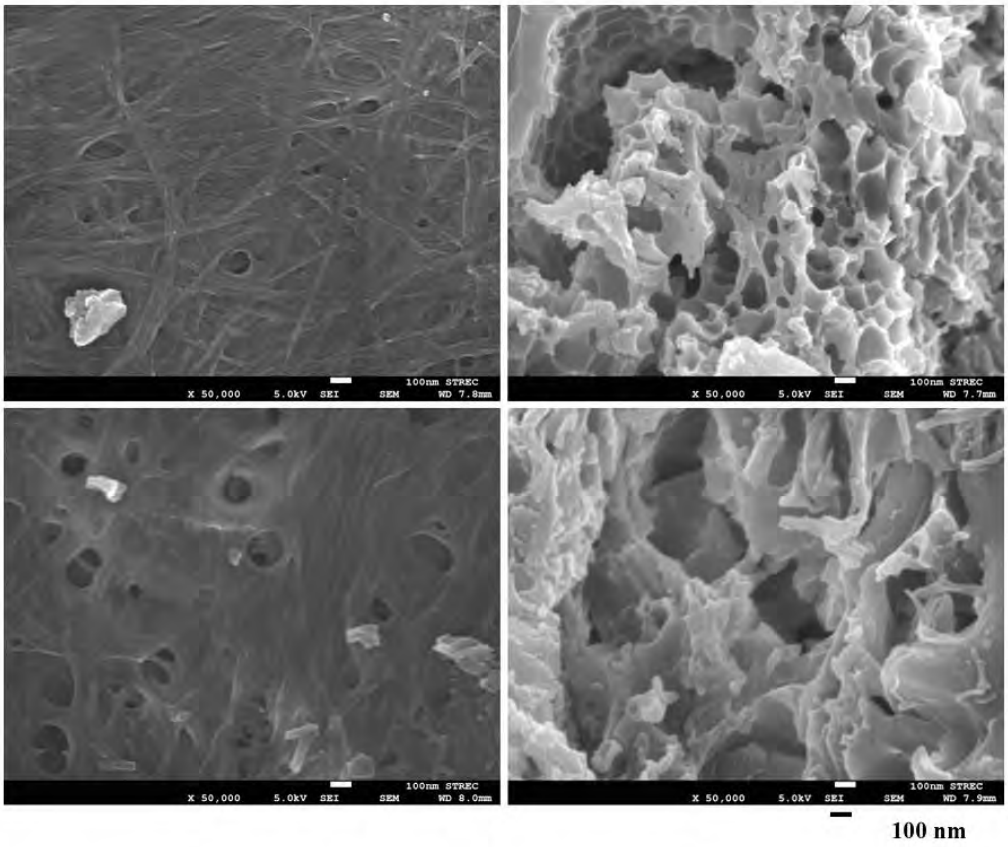

Fig. 2 Higher-magnification views of surface morphology (*left*) and cross section (*right*) of 25 Al/BC catalysts dehydrated by hot air-drying (*top*) and by freeze-drying (*bottom*)

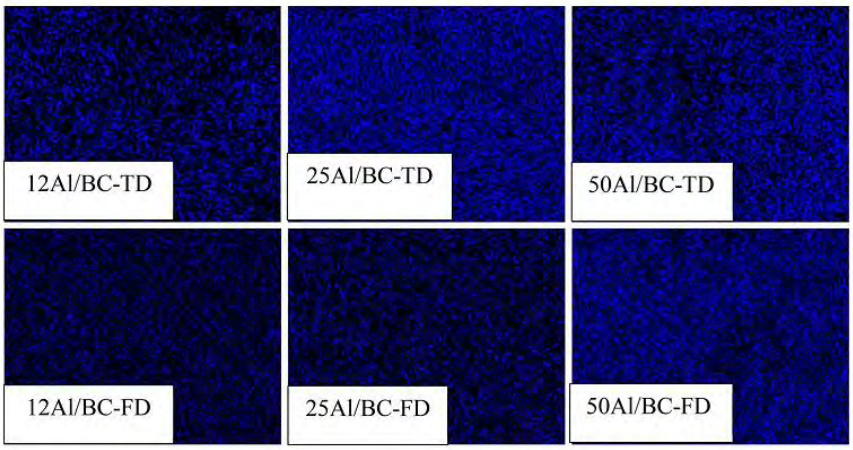

Fig. 3 EDX mapping for Al distribution on surface of Al/BC catalysts dehydrated by hot air-drying (*top*) and by freeze-drying (*bottom*)

BC > 25Al/BC > 12Al/BC, for both dehydration methods. The catalyst of 50Al/BC-TD displayed the highest total H^+ of 2158 μmol/g cat. Overall, Al/BC catalysts dehydrated by hot air drying showed slightly higher total H^+ densities than those by of freeze-drying at the same Al loading.

Table 1 Surface elemental composition obtained from energy dispersive X-ray spectroscopy and acidity of Al/BC catalysts

Catalysts	% Weight			% Atom			Total H^+ (μmol/g cat)*	Acid sites (μmol NH_3/g catalyst)**		
	C	Al	O	C	Al	O		Weak	Moderate to strong	Total
12Al/BC-TD	8.8	50.4	40.8	14.2	36.3	49.5	956	781.8	2671.6	3453.3
25Al/BC-TD	5.5	50.5	44.1	8.9	36.8	54.2	1621	567.1	2438.6	3005.7
50Al/BC-TD	6.2	60.4	33.5	10.6	46.2	43.2	2158	248.0	5342.9	5591.0
12Al/BC-FD	31.5	19.5	49.0	40.9	11.3	47.8	848	NA	NA	NA
25Al/BC-FD	23.9	36.2	39.9	34.2	23.0	42.8	1417	568.6	883.4	1452.0
50Al/BC-FD	8.0	55.7	36.4	13.2	41.3	45.5	1825	418.6	2970.1	3388.7

*Total H^+ upon the dissolution of the catalysts was determined using standard acid–base back titration

**Quantities of acid sites of catalysts were determined using Ammonia (NH_3) TPD with Fityk program calculation

The quantities of acid sites with different strength were determined by using NH_3 TPD (Table 1). The first peak observed at lower temperature (<230 °C) was due to the desorption of ammonia chemisorbed at the weak acid sites, while the higher temperature peak observed at 250–400 °C was related to moderate to strong acid sites (Figure not shown). It was revealed that the amounts of moderate to strong acid sites were higher and the amount of weak acid sites was lower with the increased loading of Al from 12 to 50%.

3.1.3 X-ray Diffraction

X-ray diffraction (XRD) was used to identify the bulk structure of the catalysts. Figure 4 shows XRD patterns of dried BC, Al/BC-TD catalysts, and Al/BC-FD catalysts. The XRD pattern of BC shows the peaks observed at 14.4°, 16.6°, and 22.4°, which are the expected peaks of BC cultured in static conditions [6, 22]. There were no regular sharp peaks of BC in the XRD patterns of all Al/BC catalysts, and the percentage of crystallinity was close to zero. Only the 12Al/BC-FD catalyst showed a broad diffraction peak around 20 at 22.5, representing amorphous carbon composed of aromatic carbon sheets [23]. These results indicate that the highly crystalline structure of BC was totally disrupted after being soaked in aluminum nitrate solution, dehydrated, and calcined. The remaining carbons from the calcination were covered by an amorphous Al coating. From the XRD analysis, all BC-supported alumina catalyst samples were fully amorphous, which is expected for alumina catalysts calcined at a low temperature.

3.1.4 Pore Structure and Surface Area

The N_2 adsorption–desorption isotherms of BC and Al/BC catalysts with various Al loadings in both dehydration processes are shown in Fig. 5. According to the International Union of Pure and Applied Chemistry classification of physisorption isotherms, the isotherms of all Al/BC catalysts

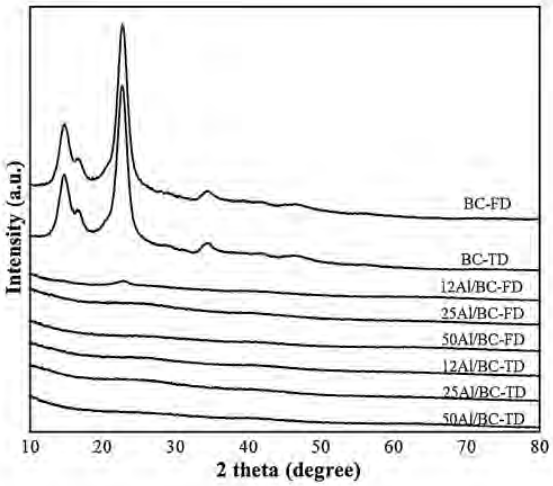

Fig. 4 XRD patterns of BC and Al/BC catalysts

were type IV, which appear as hysteresis loops at a high pressure. All the catalysts display a mesoporous structure. The Al loading content and dehydration method affected the porous structure in terms of surface area, pore volume, and pore diameter. The Brunauer–Emmett–Teller surface areas, pore volumes, and pore size diameters of dried BC, Al/BC-TD catalysts, and Al/BC-FD catalysts are summarized in Table 2. Pore size distributions of BC and Al/BC catalysts from both dehydration methods are shown in Fig. 6. The total pore volume and Brunauer–Emmett–Teller surface area decreased with increasing Al loading. The surface area decreased from 19.21 to 10.50 m^2/g and from 63.82 to 15.96 m^2/g with increasing amount of Al loading from 0 to 50 wt% on Al/BC catalysts dehydrated by hot air drying and freeze-drying, respectively. The mean pore diameters were to some extent influenced by the different dehydration methods. Al/BC catalysts dehydrated by the hot air drying method showed lower surface areas and smaller pore diameters than those of the freeze-drying

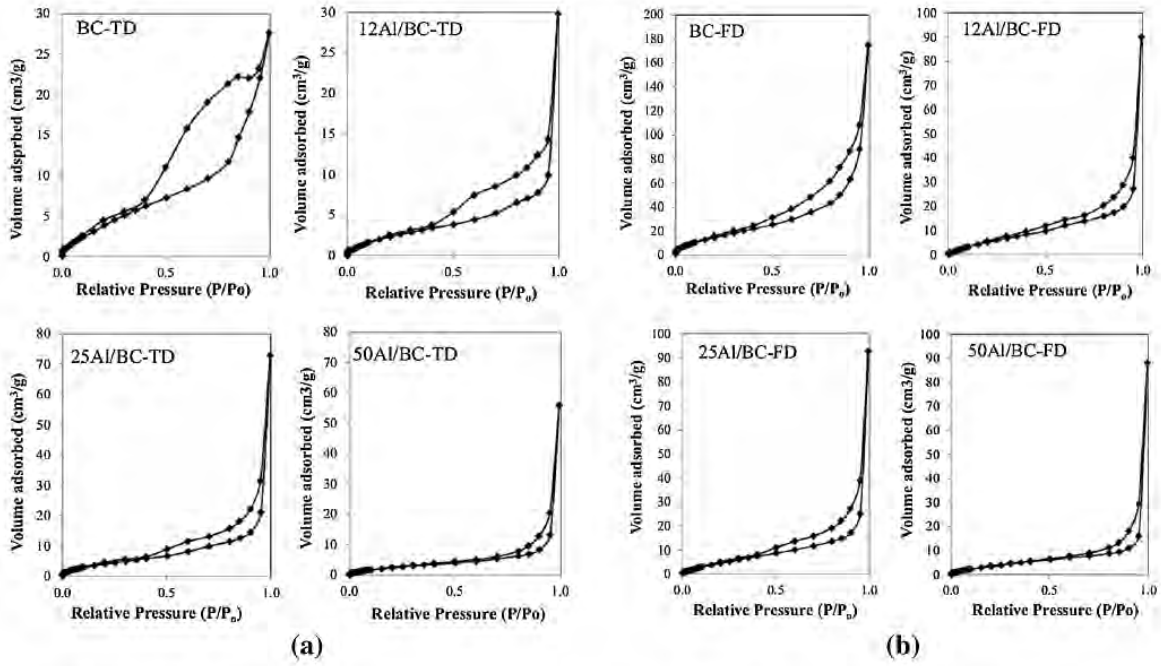

Fig. 5 The N_2 adsorption–desorption isotherms of BC and Al/BC catalysts dehydrated by hot air-drying (**a**) and freeze-drying (**b**)

Table 2 Surface area, pore volume, and average pore diameter of calcined BC particles and Al/BC catalysts determined by nitrogen adsorption and desorption (BET)

Catalysts	Surface area (m^2/g)	Total pore volume (cm^3/g)	Average pore diameter (nm)
BC-TD	19.21	0.043	8.92
12Al/BC-TD	10.47	0.046	17.67
25Al/BC-TD	17.67	0.093	25.57
50Al/BC-TD	10.50	0.087	33.01
BC-FD	63.82	0.271	16.97
12Al/BC-FD	20.07	0.140	20.62
25Al/BC-FD	21.92	0.144	26.26
50Al/BC-FD	15.96	0.137	34.25

method. In addition, significantly higher total pore volumes were obtained by dehydration via freeze-drying. All Al/BC catalysts showed average pore diameters of 17–34 nm, which were larger than that of BC without Al loading. A few micro and macro pores were also detected (Figs. 2, 6). The average pore diameter was increased with an increase of Al loading content, which was in the order: 50Al/BC > 25Al/BC > 12Al/BC > BC, for either the catalysts dehydrated by hot air drying or freeze-drying. The result indicated that the partial hydrolysis of BC might occur during the processes of soaking in the acid solution of $Al(NO_3)_3$ and calcination, resulting in increased pore

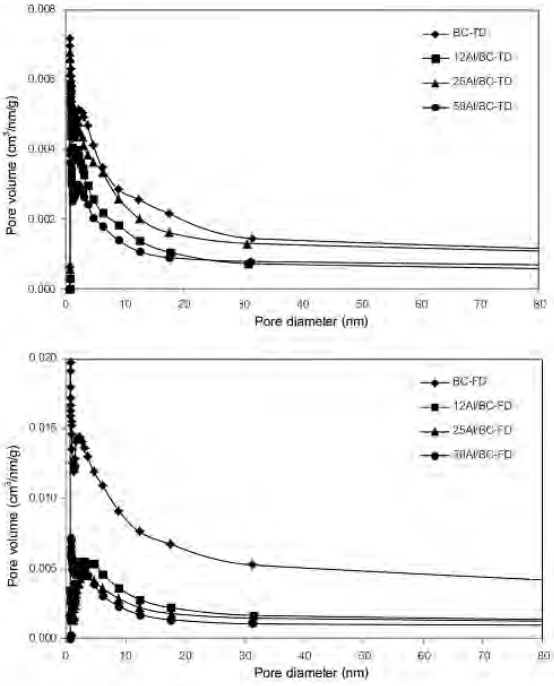

Fig. 6 BJH pore size distribution of BC and Al/BC catalysts dehydrated by hot air-drying (*top*) and freeze-drying (*bottom*)

diameters. The destruction of small pores or combination of small pores into larger pores during doping and calcination processes was previously reported [24].

3.1.5 *Fourier Transform Infrared Spectroscopy*

Fourier transforms infrared spectroscopy is often used to determine functional groups or chemical bonds in a material [25]. Figure 7 shows the infrared spectra of Al/BC-TD and Al/BC-FD catalysts with various Al loadings. The spectra of all catalyst samples were detected at wavenumbers ranging 4000–500 cm^{-1}. The infrared patterns of Al/BC-TD catalysts were similar to those of Al/BC-FD for the same concentrations of Al $(NO_3)_3$ soaking solution. The broad band located around 3380 cm^{-1} is attributed to the O–H stretching vibration of hydroxyl groups. The band at 2962 cm^{-1} is attributed to C–H interaction at the carbon surface. The sharp bands located at 2362 and 2161 cm^{-1} are attributed to the C≡C stretching vibrations of alkyne groups. However, those bands were unclear in 50Al/BC-TD and 50Al/BC-FD. The band at around 1690 cm^{-1} can be denoted as stretching C=O carbonyl groups. Moreover, the band at around 1670–1587 cm^{-1} is attributed to the C–C stretching vibration of aromatic rings and/or C=O of carboxylic groups and the bands in the region at around 1413–1300 cm^{-1} are attributed to C–O stretching vibrations. The presence of oxygen surface functional groups can be associated with the total acidity, which indicated that Al/BC catalysts were acid carbon catalysts. The results are consistent with the values of total acidity obtained by acid–base back titration (Table 1).

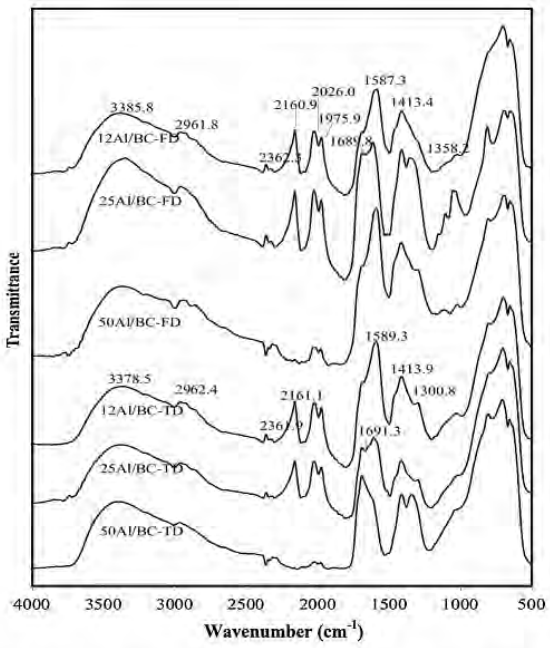

Fig. 7 The FT-IR spectra of Al/BC catalysts in wavenumber ranging from 500 to 4000 cm^{-1}

3.2 Catalytic Activity for Ethanol Dehydration

The catalytic activity of Al/BC catalysts with various Al loadings was examined in an ethanol dehydration reaction under non-oxidizing atmospheres at atmospheric pressure in the range of 200–400 °C. The dehydration products were ethylene, DEE and acetaldehyde. The ethanol conversion and selectivity for ethanol dehydration depend on the reaction temperature [26, 27]. The selectivities of ethylene and DEE, and ethanol conversion of all Al/BC catalysts are shown in Fig. 8a–c, respectively. As an endothermic reaction, the ethylene production favors high temperature. The catalysts exhibited the highest selectivity of ethylene for the reaction temperatures of 350–400 °C. The selectivity of acetaldehyde was also increased with increasing reaction temperature in a similar way as ethylene selectivity, however the concentration of acetaldehyde was much lower (figure not shown). Conversely, the selectivity of DEE was increased with decreasing reaction temperature because it is an exothermic reaction product. The highest selectivity of DEE was obtained at the reaction temperature of 200 °C. The similar effects of temperature on activity and selectivity of acid carbon catalysts for the ethanol dehydration reaction have been previously reported [18, 21, 28, 29].

Overall, the selectivity of ethylene in ethanol dehydration by Al/BC-TD catalysts was higher than that of Al/BC-FD catalysts. The results at the reaction temperatures of 250–350 °C show that the selectivity of ethylene decreased with an increase of Al loading content, which was in the order of 12Al/BC-TD > 25Al/BC-TD > 25Al/BC-FD > 50Al/BC-TD ≈ 50Al/BC-FD. The results agree with the general observation that the ethanol conversion to ethylene occurs on weak acid sites, while the strong acid centers can easily lead to ethylene polymerization [11, 18, 28]. However, by increasing the reaction temperature to 400 °C, all the Al/BC catalysts showed similar selectivity for ethylene at about 65–70% except for 12Al/BC-FD, which showed the low ethylene selectivity at ≈18% due to its very low Al concentration on the outer surface. Because of the more open pore structure on the surface of Al/BC-FD catalysts, the concentration of Al on the outer surface of 12Al/BC-FD was much lower than the other catalysts (Table 1). 12Al/BC-TD exhibited the highest selectivity of ethylene of approximately 73.0% at 350 °C. In opposition to the ethylene selectivity, the selectivity of DEE decreased with increasing reaction temperature. At the reaction temperatures of

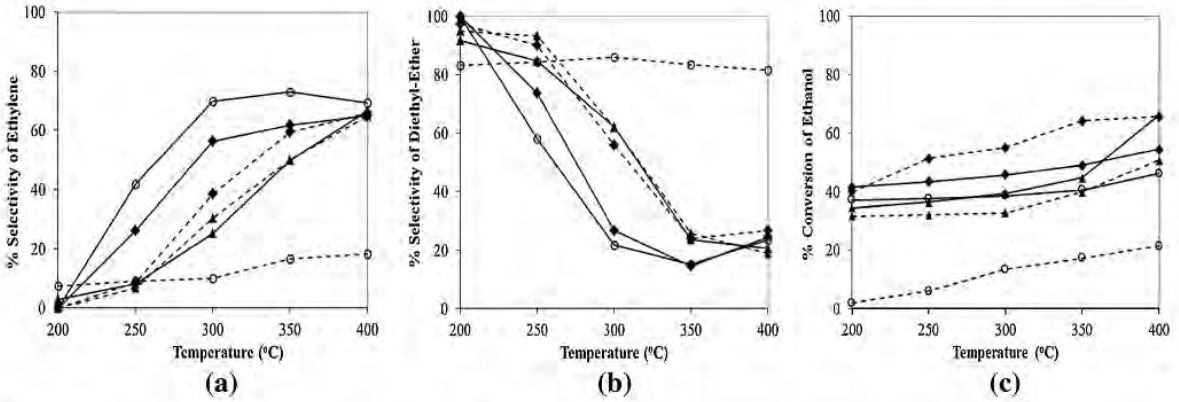

Fig. 8 Selectivity of ethylene (**a**), selectivity of diethyl-ether (DEE) (**b**) and conversion of ethanol (**c**) in ethanol dehydration at temperatures of 200–400 °C by Al/BC catalysts dehydrated by air drying (*solid line*) and freeze- drying (*dash line*) at Al loadings of 12 (*open circle*), 25 (*closed diamond*) and 50 (*closed triangle*) wt%

250 °C, the selectivity of DEE by Al/BC-FD catalysts was higher than that of Al/BC-TD catalysts and the selectivity of DEE increased with an increase of Al loading content. At 200 °C, the selectivity of all Al/BC-TD catalysts increased to 92–100%, except for the 12Al/BC-FD catalyst in which the selectivity of DEE was consistent of around 82–85% for all reaction temperatures from 200 to 400 °C. According to the selectivities of ethylene and DEE as shown in Fig. 8a, b, the reaction for ethylene production tended to occur more on the outer surface, whereas the reaction for DEE production might occur more on the inner surface of the catalysts.

Ethanol conversion by Al/BC catalysts is shown in Fig. 8c, and the catalytic performance in term of yields of ethylene, DEE, and acetaldehyde is shown in Table 3. Ethanol conversion increased with increasing reaction temperature from 200 to 400 °C. At the reaction temperature of 400 °C, the conversion of ethanol was in the order of 50Al/BC > 25Al/BC > 12Al/BC. The similar effects of temperature and the acidity of catalysts on the conversion of ethanol were previously reported [29]. The highest ethanol conversion at 66.4%, with ethylene, DEE, and acetaldehyde selectivity of 66.6, 20.7, and 12.7%, respectively, was obtained from the use of 50Al/BC-TD catalyst at 400 °C. The Al/BC catalyst with 25 wt% of Al loading and dehydration by freeze-drying (25Al/BC-FD) exhibited the highest surface area and pore volume, which were 21.92 m^2/g and 0.144 cm^3/g, respectively. At high operating temperatures (400 °C), the 25Al/BC-FD catalyst provided a similar conversion of ethanol and ethylene yield to those of the 50Al/BC-TD catalyst. However, 25Al/BC-FD catalyst showed a much higher ethanol conversion than 50Al/BC-TD catalyst at lower temperatures (200–350 °C). In addition, at low temperature of 200 °C, the catalyst of 25Al/BC-FD provided a high ethanol conversion of 40.1% with the selectivity of DEE of 97.3%. Among all Al/BC catalysts, the catalysts of 25Al/BC-FD and 50Al/BC-TD exhibited the highest ethylene yields of 43.26–44.24% at 400 °C, whereas 25Al/BC-TD and 25Al/BC-FD catalysts exhibited the highest DEE yields of 40.02–41.60% at 200 °C. Consequently, 25Al/BC-FD is considered as the promising catalyst for ethanol dehydration for both ethylene and DEE production, which could be owing to a more open porous structure with a uniform distribution of Al in the 25Al/BC-FD catalyst. The concentration of Al on the surfaces plays an important role in ethanol conversion and selectivity. Al doping at

Table 3 Yields of ethylene, diethyl ether (DEE), and acetaldehyde (MeCHO) from the dehydration of ethanol at 200, 300, and 400 °C

Catalysts	200 °C			300 °C			400 °C		
	Ethylene	DEE	MeCHO	Ethylene	DEE	MeCHO	Ethylene	DEE	MeCHO
12Al/BC-TD	0.00	37.17	0.00	27.51	8.56	3.15	32.02	10.90	3.32
25Al/BC-TD	0.00	41.60	0.00	25.77	12.31	7.76	35.36	13.36	5.82
50Al/BC-TD	0.00	31.77	1.71	9.98	24.45	4.94	44.24	13.77	8.42
12Al/BC-FD	0.16	1.78	0.19	1.37	11.64	0.52	3.96	17.66	0.00
25Al/BC-FD	1.13	40.02	1.09	21.24	30.85	3.01	43.26	17.62	4.82
50Al/BC-FD	0.00	30.18	1.57	10.01	20.35	2.46	32.94	9.57	8.22

too low concentration, especially on a highly porous support (12Al/BC-FD) caused a slow reaction, resulting in low ethanol conversion and low selectivity of ethylene. On the other hand, Al doping at very high concentration could lead to a lower overall surface area, resulting in a reduction of ethanol conversion.

In comparison with differently modified Al-based solid acid catalysts using other supports [18, 21, 28] in the same operating condition (Table 4), at high temperature operation (400 °C) the Al/BC catalysts show a lower ethanol conversion and lower ethylene yield, which could be due to the difference in form and species of alumina and its lower surface area. However, at low temperature operation (200 °C), a significantly higher ethanol conversion and higher DEE yield (DEE selectivity ≈ 100%) were obtained using 25Al/BC-TD and 25Al/BC-FD catalysts as compared with those using other Al-based solid acid catalysts [18, 21, 28]. This should be due to the interior meso–macro porous structure porous of the Al/BC catalyst. Due to the higher molecular size of DEE (MW of DEE = 74 or about 2.64 times of ethylene), the use of catalysts with small pores could limit the diffusion of DEE out of the catalyst particles. Consequently, the accumulation of DEE within the catalyst particles could limit the formation of DEE. Therefore, the porous structure of the catalyst could be one of important factors affecting the yield and selectivity of the products. In consideration of the stability of the catalysts, under a nonoxidative environment, carbon as a catalyst support can be resistant to high temperature. The structure carbon support in catalytic applications is stable at high temperatures under nonoxidative conditions (even above 726 °C) [30]. Alumina-based catalyst is also generally accepted for good stability at high temperature [29]. The 25 Al/BC catalysts showed good stability (no significant loss in conversion) during 8 h time on stream (data not shown). However, for the study of the life time of the catalysts, further work for long-term stability test should be carried out.

DEE is an excellent compression ignition fuel with higher energy density and is recently reported for the potential use as a low-emission, high-quality diesel fuel replacement. The main reaction to produce DEE from ethanol is exothermic, reversible and limited by equilibrium. With the use of Al/BC catalyst, DEE can be produced from ethanol at low temperature (200 °C) with the DEE selectivity of almost 100%. The reaction for DEE production requires much less energy than ethylene production. Therefore, for an alternative use of ethanol as a feedstock, this process would potentially provide economic and environmental benefits to the industry. Additionally, the performance of Al/BC catalyst can be further improved by optimizing the operating conditions, modifying Al/BC catalyst in terms of porous structure to enhance the surface area or improving catalytic activity by loading with more appropriate type and form of catalysts and/or adding promotors. In view of a simple, low cost, and low energy preparation method, the Al/BC catalysts are attractive for further development as an environmentally friendly catalyst for ethanol dehydration, especially for DEE production.

4 Conclusions

The supported alumina catalyst derived from BC was prepared by soaking purified BC hydrogel in $Al(NO_3)_3$ aqueous solution with various concentrations, dehydrated by hot air drying or freeze-drying and calcination in air at 200 °C for 4 h. The Al/BC catalysts reveal interior meso–macro porous structures with average pore diameters in the range of 17–34 nm. The distribution of Al on the outer surface of BC support was uniform. The increase in Al loading content from 12 to 50% increased moderate to strong acid sites, but decreased weak acid site. The Al/BC catalysts dehydrated by the freeze-drying method show higher surface area and pore volume than those by hot air drying. Increasing Al loading on BC/Al catalysts caused an increase in

Table 4 Comparison of catalysts for ethanol dehydration and their catalytic ability

Catalysts	Surface area (m^2/g)	Pore diameter (nm)	Reaction temperature (°C)	Ethanol conversion (%)	Ethylene yield (%)	DEE yield (%)	Refs
25Al/BC-TD	18	25.6	200–400	41.5–54.6	0.0–35.4	41.6–13.4	This work
25Al/BC-FD	22	26.3	200–400	41.3–65.7	1.1–43.3	40.0–17.6	This work
Al-com	137	3.9	200–400	0–95	0.0–71.3	0.0–0.0	[18]
Al-SG	152	3.5	200–400	15–98	6.8–78.4	7.0–0.0	[18]
Al-SV	215	9.3	200–400	10–100	2.5–100	7.5–0.0	[18]
Al-SSP	443.6	5.9	200–400	20–85	18.6–82.0	1.4–0.0	[28]
HBZ	522	2.2	200–400	7–100	0.0–99.4	7.1–0.0	[21]
Al-HBZ	306	3.4	200–400	9–92	0.0–90.2	9.5–1.8	[21]
M-Al	195	9.0	200–400	12–92	0.0–88.9	12.5–2.5	[21]

the pore size and a decrease in the surface area. The Al/BC catalysts show efficient dehydration of ethanol to ethylene and DEE. The highest ethanol conversion of 65.7–66.4% and ethylene yield of 43.26–44.24% were obtained by using 25Al/BC-FD or 50Al/BC-TD catalysts at a reaction temperature of 400 °C, whereas the highest DEE yield of 40.02–41.60% was obtained using 25Al/BC-FD or 25Al/BC-TD catalysts at 200 °C. It can be concluded that the acidic properties, distribution and pore structure of catalysts significantly affect the conversion of ethanol dehydration and selectivity of the reaction. The results demonstrate that BC supported Al catalyst has many promising properties, such as good metal dispersion, high chemical and thermal stabilities. In the viewpoint of eco-friendly and sustainable green chemistry, it is interesting to explore the applicability of BC-supported catalyst in various types of heterogeneous catalysis.

Acknowledgements The authors thank the Grant for International Research Integration: Chula Research Scholar, Ratchadaphiseksomphot Endowment Fund, and the National Research Council of Thailand (NRCT) for their financial support of this project.

References

1. Bailón-García E, Maldonado-Hódar FJ, Pérez-Cadenas AF, Carrasco-Marín F (2013) Catalysts 3:853
2. Zhang T, Zhao J, Xu J, Xu J, Di X, Li X (2016) Chin J Chem Eng 24:484
3. Klemm D, Heublein B, Fink HP, Bohn A (2005) Angew Chem Int Ed 44:3358
4. Xu Y, Zhang L, Cu Y (2008) J Appl Polym Sci 110:2996
5. Kanjanamosit N, Muangnapoh C, Phisalaphong M (2010) J Appl Polym Sci 115:1581
6. Phomrak S, Phisalaphong M (2017) J Nanomater. doi:10.1155/2017/4739793
7. Yang JZ, Yu J, Fan J, Sun DP, Tang WH, Yang X (2011) J Hazard Mater 189:377
8. Bedia J, Barrionuevo R, Rodriguez-Mirasol J, Corderoj T (2011) Appl Catal B 103:302
9. Fan D, Dai D-J, Wu H-S (2013) Materials 6:101
10. Huang L-D (2005) China Chlor-Alkali 5:1
11. Zhang M, Yu Y (2013) Ind Eng Chem Res 52:9505
12. Bi J, Guo X, Liu M, Wang X (2010) Catal Today 149:143
13. Han Y, Lu C, Xu D, Zhang Y, Hu Y, Huang H (2011) Appl Catal A 396:8
14. El-Katatny EA, Halawy SA, Mohamed MA, Zaki MI (2000) Appl Catal A 199:83
15. Liu D, Yao C, Zhang J, Fang D, Chen D (2011) Fuel 90:1738
16. Matsumura Y, Hashimoto K, Yoshida S (1989) J Catal 117:135
17. Takahashi R, Sato S, Sodesawa T, Arai K, Yabuki M (2005) J Catal 229:24
18. Wannaborworn M, Praserthdam P, Jongsomjit B (2015) J Nanomater 2015:1
19. Knözinger H (1968) Angew Chem Int Ed 7:791
20. Daniell W, Schubert U, Glockler R, Meyer A, Noweck K, Knozinger H (2000) Appl Catal A 196:247
21. Kamsuwan T, Jongsomjit B (2016) Eng J 20:63
22. Phisalaphong M, Suwanmajo T, Sangtherapitikul P (2008) J Appl Polym Sci 107:292
23. Kitano M, Arai K, Kodama T, Kousaka T, Nakajima K, Hayashi S, Hara M (2014) Catal Lett 131:242
24. Xiang Q, Lee YY, Pettersson PO, Torget R (2003) Appl Biochem Biotechnol 105–108:505
25. Lee YM, Kim SH, Kim SJ (1994) Polymer 37:5897
26. Lu J, Liu Y, Li N (2011) J Nat Gas Chem 20:423
27. Ouyang J, Kong F, Su G, Hu Y, Song Q (2009) Catal Lett 132:64
28. Chanchuey T, Autthanit C, Jongsomjit B (2016) J Chem 2016:96730
29. Chen G, Li S, Jiao F, Yuan Q (2007) Catal Today 125:111
30. Lam E, Luong JHT (2014) ACS Catal 4:3393

BNC2017
The 3rd Symposium on Bacterial Nanocellulose

Characteristics of activated carbon derived from bacterial cellulose and its application as a adsorbent for methylene blue adsorption

Arnon Khamkeaw and Muenduen Phisalaphong*

Chemical Engineering Research Unit for Value Adding of Bioresources, Department of Chemical Engineering, Faculty of Engineering, Chulalongkorn University, Phayathai Rd., Patumwan, Bangkok, 10330, Thailand.

*E-mail: muenduen.p@chula.ac.th

Abstract

Bacterial cellulose (BC) was investigated as a novel material for preparing activated carbons. BC was dried by heating and it was carbonized with a chemical activation process using phosphoric acid (H_3PO_4) as an activating agent at different temperatures (400, 500 and 600 °C). The properties of the activated carbons were characterized by X-ray diffraction (XRD), scanning electron microscopy (SEM), N_2-physisorption, Fourier transform infrared spectroscopy (FT-IR) and thermal gravimetric (TGA). The obtained BC activated carbons at carbonization temperature of 500°C (BC-AC500) showed maximum BET surface area (1,734 m^2/g) with mesoporous structure (2.33 nm) and large pore volume (1.01 cm^3/g). In addition, the BC-AC500 was used as adsorbent for the adsorption of methylene blue (MB). The equilibrium adsorption data were analyzed by the Langmuir, Freundlich, and Redlich-Peterson isotherm models. The results showed that the Redlich-Peterson model was found to be most fitted to the equilibrium data with correlation coefficient (R^2) value of 1. The maximum adsorption capacity (q_m) was 505.8 mg/g. The experimental results indicated that the BC activated carbon has the potential to be used as an effective adsorbent.

Keywords: activated carbon, bacterial cellulose, chemical activated carbon, adsorption, methylene blue.

ภาคผนวก(Appendix) 3

Activated carbon from bacterial cellulose as an effective adsorbent for removing dye from aqueous solution

Arnon Khamkeaw[1], Bunjerd Jongsomjit[2], Jonah Robison[1,3] and Muenduen Phisalaphong[1,*]

[1]Chemical Engineering Research Unit for Value Adding of Bioresources, [2]Center of Excellence on Catalysis and Catalytic Reaction Engineering, Department of Chemical Engineering, Faculty of Engineering, Chulalongkorn University, Phayathai Rd., Patumwan, Bangkok, 10330, Thailand. [3]Department of Bioengineering, Clemson University, Clemson SC 29634.

*Correspondence: Muenduen.p@chula.ac.th; Tel.: +662-218-6875; Fax: +662-218-6877

Abstract

The present study was conducted with the preparation of novel activated carbon from bacterial cellulose (BC) through one-step chemical activation using phosphoric acid (H_3PO_4). The AC derived from BC (BC-AC) contained over 70% of carbon with the yield of AC at 26.4%–40.2%. Carbonization at 500 °C produced mesoporous BC-AC with an average pore diameter of 2.33 nm, a surface area of 1,734 m^2/g and total pore volume of 1.01 cm^3/g. It could be used as an effective adsorbent for removing methylene blue from aqueous solutions with the maximum adsorption capacity of 505.8 mg/g.

Keywords:

Activated carbon; Bacterial cellulose; Adsorption; Methylene blue

1. Introduction

Bacterial cellulose (BC) produced by *Acetobacter xylinum* has received much attention in recent years as a renewable material with desirable properties. *A. xylinum* is a non-photosynthetic organism that can convert c-sources, such as glucose, sugar and glycerol, into pure nanocellulose [1]. BC has the same chemical structure as plant cellulose, but has a uniform nanofiber network structure and unique properties, including high crystallinity, porosity and surface area for absorption, water holding capacity, tensile strength, and resistance to organic solvents [2–4]. BC has been used in a wide range of applications, including raw material in food industries, a reinforcing agent for paper and biocompatible material for biomedical applications [5,6]. Because of its advantageous properties, BC should have great potential to be used as a source material for highly efficient activated carbon (AC) adsorbents. Previously, BC has been pyrolyzed at 950 °C and physically activated with carbon dioxide to produce active nanosized carbon for electric double-layer capacitors [7]. Recently, BC was modified with AC, amino groups, and ferriferrous oxide covered by silica to develop an adsorbent for lead ions and methyl orange from aqueous solution [8]. However, there have been very few studies conducted on the development, characterization, and evaluation of AC adsorbents derived from BC to date.

Generally, AC is prepared by either a physical or chemical process. The physical activation process involves two steps: carbonization and activation, which requires a high temperature. Chemical activation has advantages over physical activation. The required temperature is lower, it produces a higher yield of AC with higher surface, and usually involves only one step [9]. Either strong acid or strong base can be used for chemical activation. Chemicals used for the activation can lead to final materials with different porous structures based on the results from dehydration and degradation of the carbon substances.

Phosphoric acid (H_3PO_4) is a non-toxic acid commonly used as an activating agent [9]. The use of H_3PO_4 can provide high AC yield, surface area and pore volume.

Methylene blue (MB) was initially used as a dye in the textile industry. However, MB can lead to water pollution, burn the eyes of humans and animals, and cause long-term health problems. On inhalation, MB can lead to difficulty breathing for a short period of time. Upon ingestion, MB can cause nausea, sweating, vomiting, and mental confusion [10]. Adsorption is the most common process used to treat of dye-containing wastewater [11] and AC is one of the most important materials used in adsorption processes. Generally, AC is produced from carbonaceous materials such as coconut shell, rice husk, and rice bran. The physical and chemical properties of AC can depend on the materials it is derived from.

This study focuses on the development of nanoporous AC adsorbents derived from BC (denoted BC-AC) by H_3PO_4 activation at different carbonization temperatures. The produced BC-AC samples are then used as adsorbents for MB. The adsorption characteristics of the BC-AC samples are evaluated by the Langmuir, Freundlich, and Redlich–Peterson isotherm models.

2. Materials and methods

2.1. Materials

BC (Figure 1) was used as the raw material to prepare AC. BC was synthesized by *A. xylinum* AGR 60. MB used as an adsorbate was purchased from Ajax Finechem Pty. Ltd., Australia. MB has the chemical formula $C_{16}H_{18}N_3SCl$ and a molecular weight of 319.86 g/mol. The chemical structure of MB is shown in Figure 2.

2.2. Preparation of BC-ACs

The activation of BC was conducted as follows. Dried BC was mixed with H_3PO_4 at a ratio of 1:1 (w/w) and then dried in a general electric oven (SNOL 67/350 LSP01, SNOL,

Lithuania) at 110 °C for 24 h. The dried products were placed in a furnace (CWF 1100, Carbolite, UK) and carbonized at a temperature of 400, 500, or 600 °C without gas purging for 1 h before cooling. The obtained ACs were washed sequentially with 1 M HCl solution under mild stirring (120 rpm) at 70 °C for 4 h before being rinsed with distilled water several times (until the pH was 7.0) to remove residual chemicals. The samples were then dehydrated at 110 °C for 24 h. The BC-AC products obtained from carbonization at 400, 500, and 600 °C are denoted as BC-AC400, BC-AC500, and BC-AC600, respectively. The yield of AC was calculated using Eq. 1,

$$\%\,\text{Yield} = \frac{W_f}{W_0} \times 100\,, \tag{1}$$

where W_f (g) and W_0 (g) are the weights of final BC-AC product and dried BC, respectively.

2.3. Characterizations of BC-ACs

The characterizations of BC-ACs were performed by several techniques as follows. XRD (SIEMENS D5000 X-ray diffractometer, Aubrey, USA) was performed to determine the bulk crystal structure of BC-ACs using CuK_α radiation with Ni filter in the 2θ range of 10 to 70 degree with a resolution of 0.02^o and the crystallite size was calculated from Scherrer's equation. CHN Analyzer (628 Series, LECO, Germany) was used to determine the composition of C, H, and N of BC-ACs. Fourier transform infrared (FTIR) spectroscopy (Nicolet 6700 FTIR spectrometer, Thermo Scientific, USA) was used to identify functional groups in BC-AC samples. The surface area, pore volume, and pore diameter of BC-ACs were determined by nitrogen (N_2) physisorption-desorption at liquid N_2 temperature of -196°C using a Micromeritics Chemisorb 2750 Pulse instrument (Norcross, GA, USA). Field Emission Scanning Electron Microscope and Energy Dispersive X-Ray (FESEM-EDS) Spectrometer (Model of JSM-7610F and X-MaxN 20, JEOL, USA) was used to determine the morphology of BC-ACs.

3. Adsorption studies

3.1. Adsorption capacity

BC-AC was applied as adsorbent for removing MB from aqueous solutions. Solutions of MB with various concentrations of 50–600 mg/L were prepared and adjusted to pH 7.0 with 0.1 M NaOH or 0.1 M HCl. Subsequently, BC-AC (0.02 g) was added into MB solution (40 mL) in a 100-mL Erlenmeyer flask. Each MB absorption experiment was conducted at 30 °C and 125 rpm using an incubator shaker (Innova 4330, New Brunswick Scientific, USA). For the kinetics and equilibrium studies of MB adsorption, 0.1mL of the solutions was taken at different time intervals to determine MB concentration for 6 h. The concentrations of MB in the samples were analyzed by a UV–visible spectrophotometer (UV-2450. Shimadzu, Japan) at a wavelength of 664 nm. The percentage of MB removed from the solution was calculated by Eq. 2,

$$\text{Removal}(\%) = \frac{(C_0 - C_t)}{C_0} \times 100, \quad (2)$$

where C_0 and C_t (mg/L) are the initial MB concentration (t=0) and that after time t, respectively. The amount of MB adsorbed at any time, q_t (mg/g) was calculated using Eq. 3,

$$q_t = \frac{(C_0 - C_t)V}{W}, \quad (3)$$

where V (L) is the volume of solution and W (g) is the weight of BC-AC used.

The amount of MB adsorbed at equilibrium q_e (mg/g) was calculated with Eq. 4.

$$q_e = \frac{(C_0 - C_e)V}{W}, \quad (4)$$

where C_e (mg/L) is the concentration of MB in the solution after reaching equilibrium.

3.2. Adsorption isotherm modeling

The interaction between an adsorbate and adsorbent can be described by adsorption isotherms. The equilibrium data for MB adsorption on the BC-AC samples were analyzed by the Langmuir, Freundlich, and Redlich–Peterson models.

3.2.1. Langmuir model

The Langmuir isotherm model [13] was developed from the assumption that adsorption occurs on a specific homogeneous surface containing sites with equal energy. This model has been successfully applied to monolayer adsorption. The Langmuir model is expressed by Eq. 5,

$$q_e = \frac{q_m K_L C_e}{1 + K_L C_e}, \quad (5)$$

where q_m (mg/g) is the maximum adsorption capacity per unit mass of BC-AC and K_L (L/mg) is the Langmuir adsorption constant. The essential characteristics of a Langmuir isotherm can be expressed by a dimensionless constant called the equilibrium parameter R_L [14], as shown in Eq. 6.

$$R_L = \frac{1}{1 + K_L C_0}. \quad (6)$$

The value of R_L indicates whether the adsorption is irreversible ($R_L = 0$), favorable equilibrium ($0 < R_L < 1$), linear ($R_L = 1$), or unfavorable equilibrium ($R_L > 1$) [14].

3.2.2. Freundlich model

The Freundlich model [15] was developed from the assumption that adsorption occurs at specific heterogeneous surface energies. Therefore, this model is appropriate to describe multilayer adsorption with interaction between adsorbed molecules. The Freundlich model is summarized in Eq. 7.

$$q_e = K_F C_e^{1/n_F}, \quad (7)$$

where K_F ((mg/g)/(L/mg)^{n_F}) and n_F are the Freundlich constant and heterogeneity factor, respectively. The type of adsorption is linear for $n_F = 1$, a favorable chemical process for $n_F <$

1, and a favorable physical process for $n_F > 1$ [15]. Meanwhile, the value of $1/n_F < 1$ indicates a normal Langmuir isotherm and $1/n_F > 1$ indicates cooperative adsorption.

3.2.3. Redlich–Peterson model

The Redlich–Peterson model was developed to improve the curve fitting between Langmuir and Freundlich equations. It can be used to represent adsorption equilibrium over a wide concentration range, and can be applied to either homogeneous or heterogeneous systems. The Redlich–Peterson model is shown in Eq. 8 [16],

$$q_e = \frac{K_R C_e}{1 + a_R C_e^{\beta}}, \quad (8)$$

where K_R (L/g) is the Redlich–-Peterson constant, and a_R (L/mg) and β ($0 < \beta < 1$) are constants. For $\beta = 1$, the Redlich–Peterson equation transforms to Langmuir form. When K_R and a_R are much greater than unity, the equation can transform into Freundlich form [16].

4. Results and discussion

4.1. Activated carbon characterization

The yields and elemental analyses of BC-AC samples obtained at different carbonization temperatures are shown in Table 1. The yield of AC decreased considerably with rising carbonization temperature from 400 to 600 °C due to the more efficient removal of volatile species [17]. Because a gaseous fraction is rich in hydrogen, light hydrocarbons, and tar, the carbon content in a solid fraction increases with the carbonization temperature. The amount of carbon in all BC-AC samples exceeded 70% with the yield of BC at 26-40%, indicating that BC is a suitable raw material to produce ACs in the carbonization temperature range of 400–600 °C.

The bulk crystal structure of BC-AC was determined by X-ray diffraction (XRD), as shown in Figure 3.The XRD patterns of BC cultured under static conditions commonly show

three main peaks at 14°–15°, 16°–17°, and 22°–23° originating from the ($1\bar{1}0$), (110), and (200) planes, respectively (data not shown), which can be identified as the reflection planes of cellulose I [2,18,19]. The crystallinity of BC is usually between 75% and 90% [2,18]. After carbonization, the highly crystalline structure of BC was disrupted. The XRD patterns of all BC-AC samples were consistent with that of amorphous carbon derived from cellulose [20]. The XRD profiles of BC-AC samples produced at various carbonization temperatures were similar. All the BC-AC samples only displayed a diffraction peak at around 25°, which was ascribed to amorphous carbon composed of aromatic carbon sheets [21].

The chemical structures of BC-AC samples produced at various carbonization temperatures were determined by FT-IR spectroscopy; the spectra are shown in Figure 4. The broad band located around 3200–3700 cm^{-1} is attributed to the O-H stretching vibration of the hydroxyl group, which originated from the adsorption of water vapor from the surroundings and moisture residue during the carbonization process. The bands at 1600 and 1230 cm^{-1} are as ascribed to the C=O and C-O stretching vibrations of carbonyl groups, respectively, originating from the oxidative decomposition of organic species [22]. Comparison with previous reports [23-25] indicated that the broad bands are quite similar to ACs derived from many different biomass sources, with the presence of the same functional groups. The bands in the range of 1000–1200 cm^{-1} are characteristic of phosphorous and phosphor carbonaceous compounds originating from the phosphoric acid activation step. The band at 1100 cm^{-1} is ascribed to the stretching vibration of hydrogen-bonded P=O groups from phosphates or polyphosphates, O-C stretching vibrations in P-O-C (aromatic) linkages, and P=OOH [26]. The band that appears at 1000 cm^{-1} is ascribed to the ionized linkage P^{+}-O^{-} in acid phosphate esters and symmetrical vibration in a P-O-P chain [27]. The bands at 885 and 830 cm^{-1} are assigned to C-H stretching of aromatic compounds [28].

The porosity, pore volume, pore size, and specific surface area of the BC-AC samples produced at various carbonization temperatures determined by the N_2 physisorption technique are presented in Table 2. Pore size distributions of the prepared BC-ACs are shown in Figure 5. The BC-AC samples had mesoporous structures with average pore diameters in the range of 2.2–2.4 nm, which is similar to those of other ACs derived from cellulosic materials using phosphoric acid as an activating agent [31,32]. The BET surface area and total pore volume of BC-AC increased with carbonization temperature from 400 to 500 °C. In contrast, the BET surface area and total pore volume decreased slightly with rising carbonization temperature from 500 to 600 °C. It was previously reported that if the carbonization temperature is too high, the shrinkage and/or partial collapse of the carbon structure could occur and lead to decreases of the surface area and pore volume of AC products [29]. BC-AC500 had the maximum BET surface area of 1734.2 m^2/g with an average pore diameter of 2.33 nm and a total pore volume of 1.01 cm^3/g. The BC-AC samples demonstrated higher relative BET surface area and total pore volume than those of ACs derived from cotton stalk [30], deoiled rice bran residue [31], and durian shell [32]. The surface area and total pore volume of BC-AC500 were comparable to those of high surface area AC obtained from Elaeagnus angustifolia seeds by one-stage chemical activation using $ZnCl_2$ in N_2 [33]; however, the average pore size of BC-AC500 was relatively higher. According to a previous report for the preparation of AC from deoileded rice bran residues, $ZnCl_2$ activation produced AC with higher surface area and total pore volume but slightly smaller pore diameter than those from H_3PO_4 activation [31]. However, when considering safety issues, H_3PO_4 activation is widely preferred over $ZnCl_2$ activation.

The surface morphologies of the BC-AC samples were observed by FESEM, as depicted in Figure 6. The BC-AC samples exhibit rough surfaces, which are associated with

the presence of very small pores originating from the evaporation of H_3PO_4 and other volatile matter during carbonization [34].

The mass loss during thermogravimetric analysis (TGA) of BC-AC at various carbonization temperatures is shown in Figure 7. The TGA patterns of all BC-ACs are similar. The initial small mass loss from around room temperature (30 °C) to 100 °C was attributed to moisture elimination. From 100 to 500 °C, only a small amount of carbon decomposition (less than 5% of the initial weight for BC-AC400 and BC-AC500; less than 2% of the initial weight for BC-AC600) was detected, indicating that the BC-AC samples exhibited high stability between 0 and 500 °C.

4.2. Adsorption capacity: effects of contact time and initial MB concentration

Figure 8 shows the effects of contact time and initial MB concentration on the adsorption capacity of the BC-AC samples. Under the controlled conditions (in 3.1), all samples initially showed rapid adsorption rates (0 to 15 min) and then the adsorption rates gradually decreased until the equilibrium was reached. The equilibrium of MB adsorption by BC-AC400 was achieved within 20 min for the systems with low MB concentration (50 and 100 mg/L) and within 300 min for those with high MB concentration (200–600 mg/L). For BC-AC500 and BC-AC600, the time required to reach equilibrium was shorter compared with that for BC-AC400 (10 min for the systems with low MB concentration and 240 min for those with high MB concentration). The higher pore volume and surface area of BC-AC500 and BC-AC600 (as compared to those of BC-AC400) could promote the diffusion of MB molecules from the bulk solution into the interior of the adsorbents. In addition, in the systems with low MB concentration, the adsorbent has a high content of available vacant active sites; thus, the adsorption equilibrium could be reached faster compared with the cases of high MB concentration [10].

The maximum MB adsorption was attained using the MB solution with the highest initial MB concentration (600 mg/L), but this system also gave the lowest percent removal of MB from the solution. BC-AC600 and BC-AC500 had very high adsorption capacities for MB with maximum values of 507.5 and 505.8 mg/g, respectively, whereas BC-AC400 had a lower adsorption capacity of 393.0 mg/g. The increase of the surface area of adsorbents could raise adsorption capacity by allowing more interaction between active sites and MB molecules [35]. The percent removal of MB increased with contact time until the equilibrium was reached (Figure 9). Using the BC-AC samples, complete MB removal could be achieved if the initial MB concentration did not exceed 100 mg/L. Because the concentration ratio of active sites and MB in the systems with low MB concentration is high, all MB molecules could be adsorbed on active sites of the adsorbent [36]. In addition, BC-AC400, BC-AC500, and BC-AC600 showed MB removal of 88.4%, 99.8%, and 99.8%, respectively, when the initial MB concentration was 200 mg/L. The removal of MB decreased with increasing initial MB concentration from 200 to 600 mg/L. Table 3 compares the maximum capacity (q_m) for MB adsorption by the BC-AC samples with those achieved by other AC adsorbents. The q_m values of BC-AC500 and BC-AC600 for MB adsorption are higher than those of ACs derived from other cellulosic materials (q_m ~ 90-435 mg/g), which should be because the BC-AC samples possess nanoporous structures with high porosity and surface area. The results indicated that the BC-AC samples are effective adsorbents for the removal of MB from aqueous solutions.

4.3. Adsorption isotherms

Figure 10 illustrates the non-linear fittings of the Langmuir, Freundlich, and Redlich–Peterson isotherm models for the three adsorbents, while Table 4 summarizes the corresponding isotherm parameters and their correlation coefficients (R^2) for each fitting. The q_m values for BC-AC400, BC-AC500, and BC-AC600 obtained by fitting the Langmuir

isotherm model to the equilibrium data are 383.2, 500.0, and 500.0 mg/g, respectively, which are very close to the experimental values (393.0, 505.8, and 507.5 mg/g, respectively; see Fig. 8). K_L for the samples is 0.7–10.0 L/mg, indicating that the adsorption strength is strong [44]. Meanwhile, the value of R_L could indicate the nature of the isotherm. According to Fig. 10, for the initial MB concentrations of 200–600 mg/L, R_L decreased with increasing initial MB concentration and was in the range of 2×10^{-4} to 7×10^{-3}, which indicates that the adsorption of MB by the BC-AC samples is favorable [14,45].

The n_F parameter of Freundlich isotherm of all BC-ACs in this research presented favorable physical adsorption process, while $1/n_F$ was consistent with favorable normal Langmuir isotherms [15]. Comparison of the R^2 values for all BC-AC samples between the Langmuir and Freundlich isotherms indicated that the Langmuir model fitted the experimental data better than the Freundlich model. Therefore, MB tended to be adsorbed as a monolayer by the BC-AC samples [13]. The Redlich–Paterson isotherm model was found to give the best fit of the experimental data, with an R^2 value of 1.000. The Redlich–Peterson isotherm model was combined with the Langmuir and Freundlich isotherm models. Generally, the Langmuir isotherm model is good for predicting low adsorbate concentration, whereas the Freundlich model might better describe the adsorption at high adsorbate concentration [16]. The limitation of adsorbate concentration of the Langmuir and Freundlich isotherm model could be improved by the Redlich–Peterson isotherm model, which can be used to predict a wide range of adsorbate concentrations [16]. The β values for all BC-AC samples are close to 1.0, which indicates that the Langmuir isotherm model (describing monolayer adsorption) is more appropriate than the Freundlich (describing multilayer adsorption). Overall, it can be concluded that the adsorption of MB by the BC-AC samples is mostly monolayer adsorption. Comparison of R^2 values (Table 5) indicated that the order of the models that best fit the experimental data is Redlich–Peterson > Langmuir > Freundlich.

It was previously reported that the Redlich–Peterson isotherm model showed the best fit for MB adsorption onto an AC produced from steam-activated bituminous coal over the Langmuir and Freundlich models [46].

5. Conclusion

Novel AC derived from BC was found to be effective as an adsorbent to remove MB from water. The carbonization temperature markedly affected the porous structure of the BC-AC samples. A carbonization temperature of 500 °C gave the sample that possessed the highest surface area of 1,734.2 m^2/g with a total pore volume of 1.011 cm^3/g. The BC-AC samples had a mesoporous structure with an average pore diameter of 2.2–2.4 nm and high thermal stability between 100 and 500 °C. By using BC-AC500 or BC-AC600 at 0.02 g in 40 mL MB solution for MB removal, adsorption equilibria could be reached within 10 min for systems with low MB concentration (50–100 mg/L) and 240 min for those with high MB concentration (200–600 mg/L). The removal of MB from solutions with an initial MB concentration not exceeding 200 mg/L was almost 100%. The maximum MB adsorption capacities of BC-AC400, BC-AC500, and BC-AC600 were 393.0, 505.8, and 507.5 mg/g, respectively, which were very close to the q_m values estimated from the Langmuir model. The analysis results indicated that all BC-ACs presented favorable physisorption and the adsorption of MB is most likely to be a monolayer adsorption. The Redlich–Peterson model displayed the best fit with the experimental data of the models considered, with R^2 values of 1.000 for all BC-AC samples. With its very high adsorption capacities and rate, BC-AC have high potential to be used as an effective adsorbent for water treatment systems.

Acknowledgement

The authors thank the Grant for International Research Integration: Chula Research Scholar, Ratchadaphiseksomphot Endowment Fund, and the National Research Council of Thai-land (NRCT) for their financial support of this project. The authors also acknowledge the 100th Anniversary Chulalongkorn University Fund for doctoral scholarship.

References

[1] Hestrin, S.; Schramm, M. (1954) Synthesis of cellulose by *Acetobacter xylinum*. II. Preparation of freeze-dried cells capable of polymerizing glucose to cellulose. *Biochem. J.*, 58(2): 345-352.

[2] Taokaew, S.; Seetabhawang, S.; Siripong, P.; Phisalaphong, M. (2013) Biosynthesis and characterization of nanocellulose-gelatin films. *Carbohyd. Polym.*, 6(3): 782-794

[3] Luddee, M.; Pivsa-Art, S.; Sirisansaneeyakul, S.; Pechyen, C. (2014) Particle size of ground bacterial cellulose affecting mechanical, thermal, and moisture barrier properties of PLA/BC biocomposites. *Energ. Proced.*, 56: 211-218.

[4] Çakar, F.; Özer, I.; Aytekin, A.Ö.; Şahin, F. (2014) Improvement production of bacterial cellulose by semi-continuous process in molasses medium. *Carbohyd. Polym.*, 106: 7-13.

[5] Kirdponpattara, S.; Khamkeaw, A.; Sanchavanakit, N.; Pavasant, P.; Phisalaphong, M. (2015) Structural modification and characterization of bacterial cellulose–alginate composite scaffolds for tissue engineering. *Carbohyd. Polym.*, 132: 146-155.

[6] Klemm, D.; Schumann, D.; Udhardt, U.; Marsch, S. (2001) Bacterial synthesized cellulose - artificial blood vessels for microsurgery. *Prog. Polym. Sci.*, 26(9): 1561-1603.

[7] Lee, K.-Y.; Qian, H.; Tay, F.H.; Blaker, J.J.; Kazarian, S.G.; Bismarck, A. (2013) Bacterial cellulose as source for activated nanosized carbon for electric double layer capacitors. *Journal of Materials Science*, 48(1): 367-376.

[8] Huang, X.; Zhan, X.; Wen, C.; Xu, F.; Luo, L. (2017) Amino-functionalized magnetic bacterial cellulose/activated carbon composite for Pb^{2+} and methyl orange sorption from aqueous solution. *J. Mater. Sci. Technol.*, (in press).

[9] Yahya, M.A.; Al-Qodah, Z.; Ngah, C.W.Z. (2015) Agricultural bio-waste materials as potential sustainable precursors used for activated carbon production: A review. *Renew. Sust. Energ. Rev.*, 46: 218-235.

[10] Ahmed, M.J.; Dhedan, S.K. (2012) Equilibrium isotherms and kinetics modeling of methylene blue adsorption on agricultural wastes-based activated carbons. *Fluid Phase Equilibr.*, 317: 9-14.

[11] Nagarajan, K.; Renganathan, T.; Krishnaiah, K. (2016) Dye removal in steady-state continuous countercurrent liquid–solid adsorber. *Sep Sci Technol.*, 51(12): 1955-1961.

[12] Vasanth Kumar, K.; Sivanesan, S. (2006) Equilibrium data, isotherm parameters and process design for partial and complete isotherm of methylene blue onto activated carbon. *J. Hazard. Mater.*, 134(1): 237-244.

[13] Langmuir, I. (1917) The constitution and fundamental properties of solids and liquids. *J. Frankl. Inst.*, 183(1): 102-105.

[14] Hall, K.; C. Eagleton, L.; Acrivos, A.; Vermeulen, T. (1966) Pore and solid diffusion kinetics in fixed-bed adsorption under constant-pattern. *Ind. Eng. Chem. Fundam.*, 5: 212–223.

[15] Bhatt, A.S.; Sakaria, P.L; Vasudevan, M.; Pawar, R.R.; Sudheesh, N.; Bajaj, H.C.; Mody, H.M. (2012) Adsorption of an anionic dye from aqueous medium by organoclays: equilibrium modeling, kinetic and thermodynamic exploration. *RSC Advances*, 2: 8663–8671.

[16] Omar, H. A. (2013) Adsorption of ^{60}Co on Natural and Dithizone-Modified Chitin. *Radiochemistry*, 55(1): 101–107.

[17] Bedia, J.; Barrionuevo, R.; Rodríguez-Mirasol, J.; Cordero, T. (2011) Ethanol dehydration to ethylene on acid carbon catalysts. *Appl. Catal. B-Environ.*, 103(3): 302-310.

[18] Phisalaphong, M.; Jatupaiboon, N. (2008) Biosynthesis and characterization of bacteria cellulose–chitosan film. *Carbohyd. Polym.*, 74(3): 482-488.

[19] Ibnu Abdulwahab, M.; Khamkeaw, A.; Jongsomjit, B.; Phisalaphong, M. (2017) Bacterial cellulose supported alumina catalyst for ethanol dehydration. *Catal. Lett.*, 147(9): 2462-2472.

[20] Winter, C.; Caetano, J.N.; Araújo, A.B.C.; Chaves, A.R.; Ostroski, I.C.; Vaz, B.G.; Pérez, C.N.; Alonso, C.G. (2016) Activated carbons for chalcone production: Claisen-Schmidt condensation reaction. *Chem. Eng. J.*, 303: 604-610.

[21] Djilani, C.; Zaghdoudi, R.; Modarressi, A.; Rogalski, M.; Djazi, F.; Lallam, A. (2012) Elimination of organic micropollutants by adsorption on activated carbon prepared from agricultural waste. *Chem. Eng. J.*, 189: 203-212.

[22] Finocchio, E.; Cristiani, C.; Dotelli, G.; Stampino, P.G.; Zampori, L. (2014) Thermal evolution of PEG-based and BRIJ-based hybrid organo-inorganic materials. FT-IR studies. *Vib. Spectrosc.*, 71: 47-56.

[23] Chen, Y.; Huang, B.; Huang, M.; Cai, B. (2011) On the preparation and characterization of activated carbon from mangosteen shell. *J. Taiwan Inst. Chem. E.*, 42(5): 837-842.

[24] Oliveira, L.C.A.; Pereira, E.; Guimaraes, I.R.; Vallone, A.; Pereira, M.; Mesquita, J.P.; Sapag, K. (2009) Preparation of activated carbons from coffee husks utilizing $FeCl_3$ and $ZnCl_2$ as activating agents. *J. Hazard. Mater.*, 165(1): 87-94.

[25] Shi, Q.; Zhang, J.; Zhang, C.; Li, C.; Zhang, B.; Hu, W.; Xu, J.; Zhao, R. (2010) Preparation of activated carbon from cattail and its application for dyes removal. *J. Environ. Sci.*, 22(1): 91-97.

[26] Yorgun, S.; Yıldız, D. (2015) Preparation and characterization of activated carbons from Paulownia wood by chemical activation with H_3PO_4. *J. Taiwan Inst. Chem. E.*, 53: 122-131.

[27] Yakout, S.M.; Sharaf El-Deen, G. (2016) Characterization of activated carbon prepared by phosphoric acid activation of olive stones. *Arab. J. Chem.*, 9: S1155-S1162.

[28] Pereira, R.G.; Veloso, C.M.; da Silva, N.M.; de Sousa, L.F.; Bonomo, R.C.F.; de Souza, A.O.; Souza, M.O.d.G.; Fontan, R.d.C.I. (2014) Preparation of activated carbons from cocoa shells and siriguela seeds using H_3PO_4 and $ZnCl_2$ as activating agents for BSA and α-lactalbumin adsorption. *Fuel Process.Technol.*, 126: 476-486.

[29] Armandi, M.; Bonelli, B.; Geobaldo, F.; Garrone, E. (2010) Nanoporous carbon materials obtained by sucrose carbonization in the presence of KOH. *Micropor. Mesopor. Mat.*, 132(3): 414-420.

[30] Guo, S.; Peng, J.; Li, W.; Yang, K.; Zhang, L.; Zhang, S.; Xia, H. (2009) Effects of CO_2 activation on porous structures of coconut shell-based activated carbons. *Appl. Surf. Sci.*, 255(20): 8443-8449.

[31] Niticharoenwong, B.; Shotipruk, A.; Mekasuwandumrong, O.; Panpranot, J.; Jongsomjit, B. (2013) Characteristics of activated carbons derived from deoiled rice bran residues. *Chem. Eng. Commun.*, 200(10): 1309-1321.

[32] Yee Jun, T.; Devi Arumugam, S.; Hidayah Abdul Latip, N.; Abdullah, A.; Abdul Latif, P. (2010) Effect of activation temperature and heating duration on physical characteristics of activated carbon prepared from agriculture waste. *Environ. Asia*, 3: 143–148.

[33] Şahin, Ö.; Saka, C.; Ceyhan, A.A.; Baytar, O. (2015) Preparation of high surface area activated carbon from *Elaeagnus angustifolia* seeds by chemical activation with $ZnCl_2$ in one-step treatment and its iodine adsorption. *Sep Sci Technol.*, 50(6): 886-891.

[34] Demiral, H.; Gündüzoğlu, G. (2010) Removal of nitrate from aqueous solutions by activated carbon prepared from sugar beet bagasse. *Bioresource Technol.*, 101(6): 1675-1680.

[35] Aguayo-Villarreal, I.A.; Bonilla-Petriciolet, A.; Muñiz-Valencia, R. (2017) Preparation of activated carbons from pecan nutshell and their application in the antagonistic adsorption of heavy metal ions. *J. Mol. Liq.*, 230: 686-695.

[36] Geçgel, Ü.; Özcan, G.; Gürpınar, G.Ç. (2013) Removal of methylene blue from aqueous solution by activated carbon prepared from pea shells (*Pisum sativum*). *J. Chem-Ny.*, 2013: 1-9.

[37] Tan, I.A.W.; Ahmad, A.L.; Hameed, B.H. (2008) Adsorption of basic dye on high-surface-area activated carbon prepared from coconut husk: Equilibrium, kinetic and thermodynamic studies. *J. Hazard. Mater.*, 154(1): 337-346.

[38] Attia, A.A.; Girgis, B.S.; Fathy, N.A. (2008) Removal of methylene blue by carbons derived from peach stones by H_3PO_4 activation: Batch and column studies. *Dyes Pigments*, 76(1): 282-289.

[39] Tan, I.A.W.; Ahmad, A.L.; Hameed, B.H. (2008) Enhancement of basic dye adsorption uptake from aqueous solutions using chemically modified oil palm shell activated carbon. *Colloid. Surface. A.*, 318(1): 88-96.

[40] Kannan, N.; Sundaram, M.M. (2001) Kinetics and mechanism of removal of methylene blue by adsorption on various carbons-a comparative study. *Dyes Pigments*, 51(1): 25-40.

[41] Tan, I.A.W.; Hameed, B.H.; Ahmad, A.L. (2007) Equilibrium and kinetic studies on basic dye adsorption by oil palm fibre activated carbon. *Chem. Eng. J.*, 127(1): 111-119.

[42] Sainz-Diaz, C.I.; Griffiths, A.J. (2000) Activated carbon from solid wastes using a pilot-scale batch flaming pyrolyser. *Fuel*, 79(15): 1863-1871.

[43] El-Halwany, M.M. (2010) Study of adsorption isotherms and kinetic models for Methylene Blue adsorption on activated carbon developed from Egyptian rice hull (Part II). *Desalination*, 250(1): 208-213.

[44] Zamani, S.; Tabrizi, N.S. (2015) Removal of methylene blue from water by graphene oxide aerogel: thermodynamic, kinetic, and equilibrium modeling. *Res. Chem. Intermediate*, 41(10): 7945-7963.

[45] Vučurović, V.M.; Razmovski, R.N.; Tekić, M.N. (2012) Methylene blue (cationic dye) adsorption onto sugar beet pulp: Equilibrium isotherm and kinetic studies. *J. Taiwan Inst. Chem. E.*, 43(1): 108-111.

[46] El Qada, E.N.; Allen, S.J.; Walker, G.M. (2006) Adsorption of Methylene Blue onto activated carbon produced from steam activated bituminous coal: A study of equilibrium adsorption isotherm. *Chem. Eng. J.*, 124(1): 103-110.

Table 1 Yields and elemental analysis of activated carbons (AC) derived from bacterial cellulose (BC) at various carbonization temperatures.

BC-AC	Yield (%)	Carbon (%)	Oxygen (%)	Hydrogen (%)	Nitrogen (%)
BC-AC400	40.20	70.93	25.27	2.89	0.91
BC-AC500	33.40	72.48	23.93	2.44	1.15
BC-AC600	26.36	73.67	21.95	3.55	0.83

Table 2 Porous properties of BC-ACs carbonized at temperatures of 400°C (BC-AC400), 500°C (BC-AC500), and 600°C (BC-AC600).

BC-AC	BET surface area (m^2/g)	Total pore volume (cm^3/g)	Average pore diameter (nm)
BC-AC400	1,540.1	0.87	2.25
BC-AC500	1,734.2	1.01	2.33
BC-AC600	1,701.5	1.01	2.37

Table 3 The maximum adsorption capacity for MB removal by BC-ACs in this work as compared to those by ACs derived from other cellulosic materials.

Adsorbent	q_m (mg/g)	Reference
BC-AC400	393.0	This work
BC-AC500	505.8	This work
BC-AC600	507.5	This work
Coconut husk-based AC	434.8	[37]
Peach stones-based AC	412.0	[38]
Date stone-based AC	398.2	[10]
Oil palm shell-based AC	303.0	[39]
Coconut shell-based AC	277.9	[40]
Oil palm fiber-based AC	277.8	[41]
Ground shell-based AC	164.9	[40]
Bamboo dust-based AC	150.0	[40]
Activated sewage char	120.0	[42]
Oil palm wood-based AC	90.0	[43]

Table 4 Isotherm parameters and R^2 for MB adsorption on BC-ACs analyzed by the Langmuir, Freundlich and Redlich-Peterson isotherm models.

Activated carbon	Parameters of isotherms		
	Langmuir	Freundlich	Redlich-Peterson
BC-AC400	q_m = 384.6 mg/g K_L = 0.7 L/mg R_L = 2 x 10^{-3} - 7 x 10^{-3} R^2 = 0.985	K_F = 325.3 (mg/g)/(L/mg)$^{n}_{F}$ n_F = 32.57 $1/n_F$ = 0.031 R^2 = 0.976	K_R = 326.9 L/g a_R = 1.000 L/mg β = 0.970 R^2 = 1.000
BC-AC500	q_m = 500.0 mg/g K_L =10.0 L/mg R_L = 2 x 10^{-4} - 5 x 10^{-4} R^2 = 0.984	K_F = 410.4 (mg/g)/(L/mg)$^{n}_{F}$ n_F = 28.33 $1/n_F$ = 0.035 R^2 = 0.976	K_R = 6753.0 L/g a_R = 14.53 L/mg β = 0.988 R^2 = 1.000
BC-AC600	q_m = 500.0mg/g K_L = 5.0 L/mg R_L = 3 x 10^{-4} - 10 x 10^{-4} R^2 = 0.994	K_F = 398.5 (mg/g)/(L/mg)$^{n}_{F}$ n_F = 23.64 $1/n_F$ = 0.042 R^2 = 0.923	K_R = 2280.0 L/g a_R = 4.577 L/mg β = 1.000 R^2 = 1.000

Figure Captions

Figure 1. Image of BC (a) and SEM surface morphology of BC (b).

Figure 2. Structure of methylene blue dye (MB) [12].

Figure 3. The XRD patterns of BC-ACs carbonized at temperatures of 400°C (BC-AC400), 500°C (BC-AC500), and 600°C (BC-AC600).

Figure 4. The FT-IR patterns of BC-ACs carbonized at temperatures of 400°C (BC-AC400), 500°C (BC-AC500), and 600°C (BC-AC600).

Figure 5. Pore size distribution of BC-ACs: BC-AC400 (−), BC-AC500 (---), and BC-AC600 (····).

Figure 6. FESEM micrographs of BC-ACs: BC-AC400 (a), BC-AC500 (b), and BC-AC600 (c).

Figure 7. Thermal gravimetric of BC-ACs: BC-AC400 (−), BC-AC500 (---), and BC-AC600 (····).

Figure 8. Effects of contact time and initial MB concentration (■50, ♦100, ●200, △300, □400, ◊500, and ○600 mg/L) on the adsorption capacity of BC-AC400 (a), BC-AC500 (b) and BC-AC600 (c).

Figure 9. Effects of contact time and initial MB concentration (■50, ♦100, ●200, △300, □400, ◊500, and ○600 mg/L) on the removal of MB of BC-AC400 (a), BC-AC500 (b) and BC-AC600 (c).

Figure 10. Equilibrium adsorption data of MB on different BC-ACs; BC-AC400 (a), BC-AC500 (b), BC-AC600 (c), analyzed by the Langmuir (---), Freundlich (····) and Redlich-Peterson (−) isotherms, and the equilibrium parameter R_L by the Langmuir model (d) for BC-AC400 (○), BC-AC500 (□), and BC-AC600 (△).

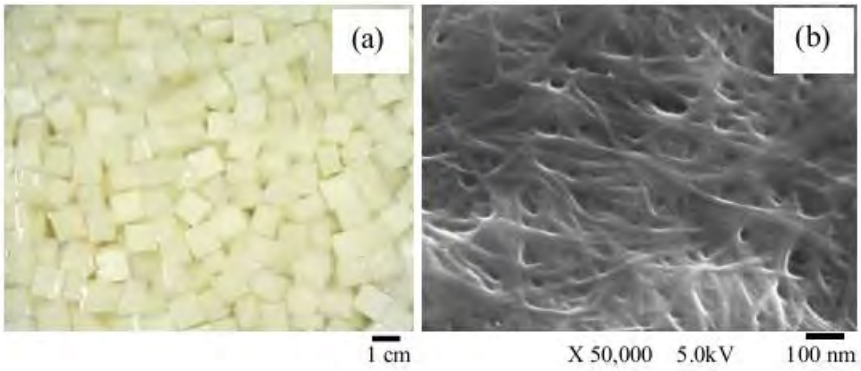

Fig. 1

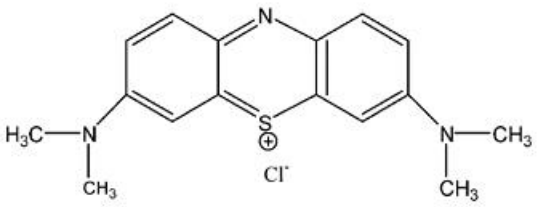

Fig. 2

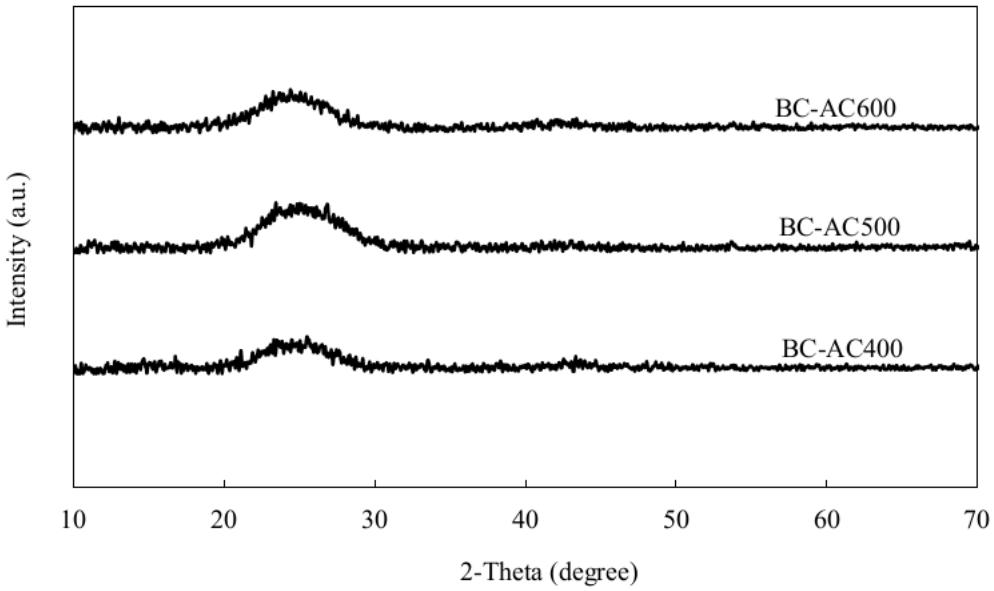
BC-AC600
BC-AC500
BC-AC400
Intensity (a.u.)
10
20
30
40
50
60
70
2-Theta (degree)

Fig. 3

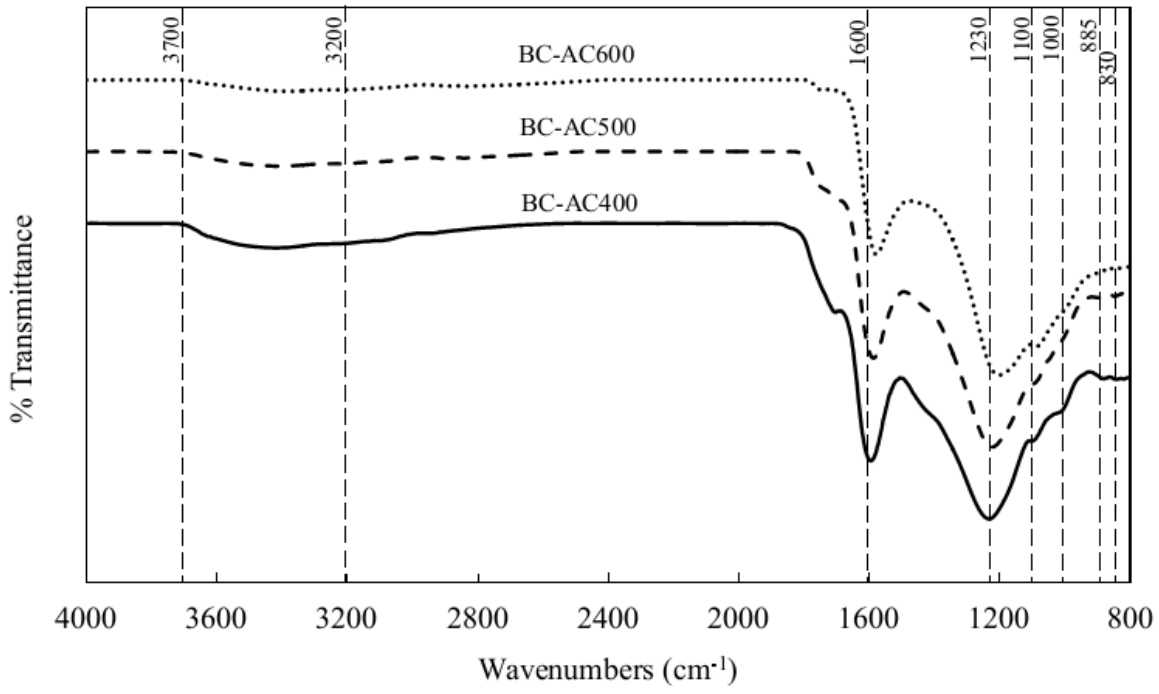
3700
3200
1600
1230
1100
1000
885
830
BC-AC600
BC-AC500
BC-AC400
% Transmittance
4000
3600
3200
2800
2400
2000
1600
1200
800
Wavenumbers (cm-1)

Fig. 4

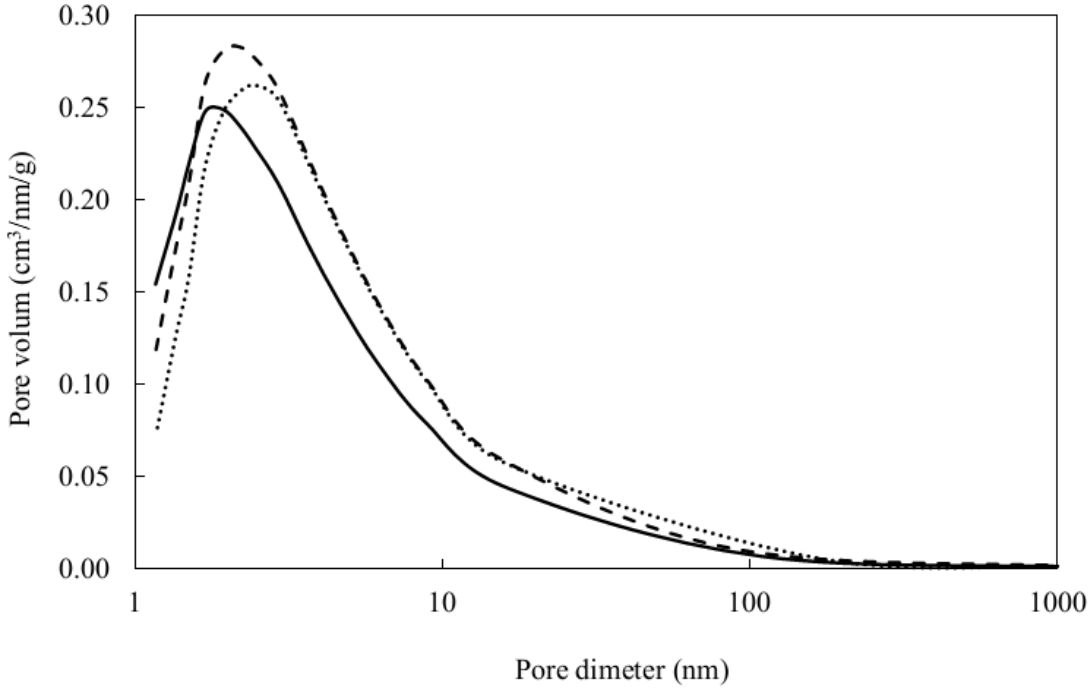
0.30
0.25
0.20
0.15
0.10
0.05
0.00
Pore volum (cm3/nm/g)
1
10
100
1000
Pore dimeter (nm)

Fig. 5

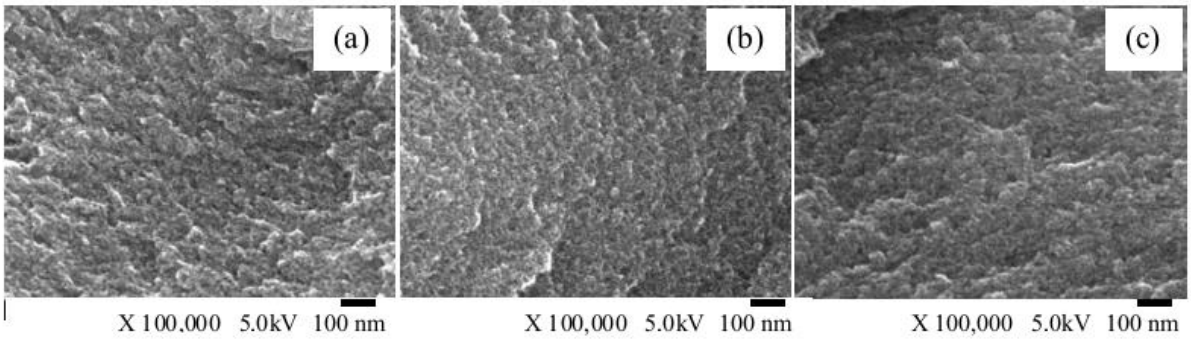
(a)
(b)
(c)
X 100,000 5.0kV 100 nm
X 100,000 5.0kV 100 nm
X 100,000 5.0kV 100 nm

Fig.6

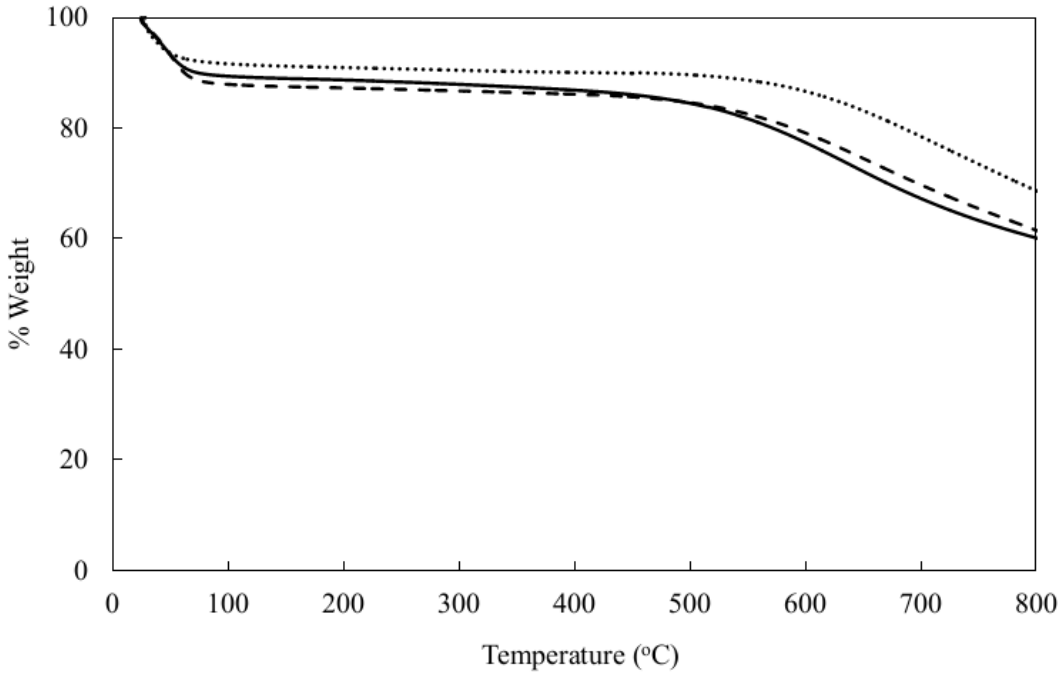
100
80
60
40
20
0
% Weight
0
100
200
300
400
500
600
700
800
Temperature (°C)

Fig. 7

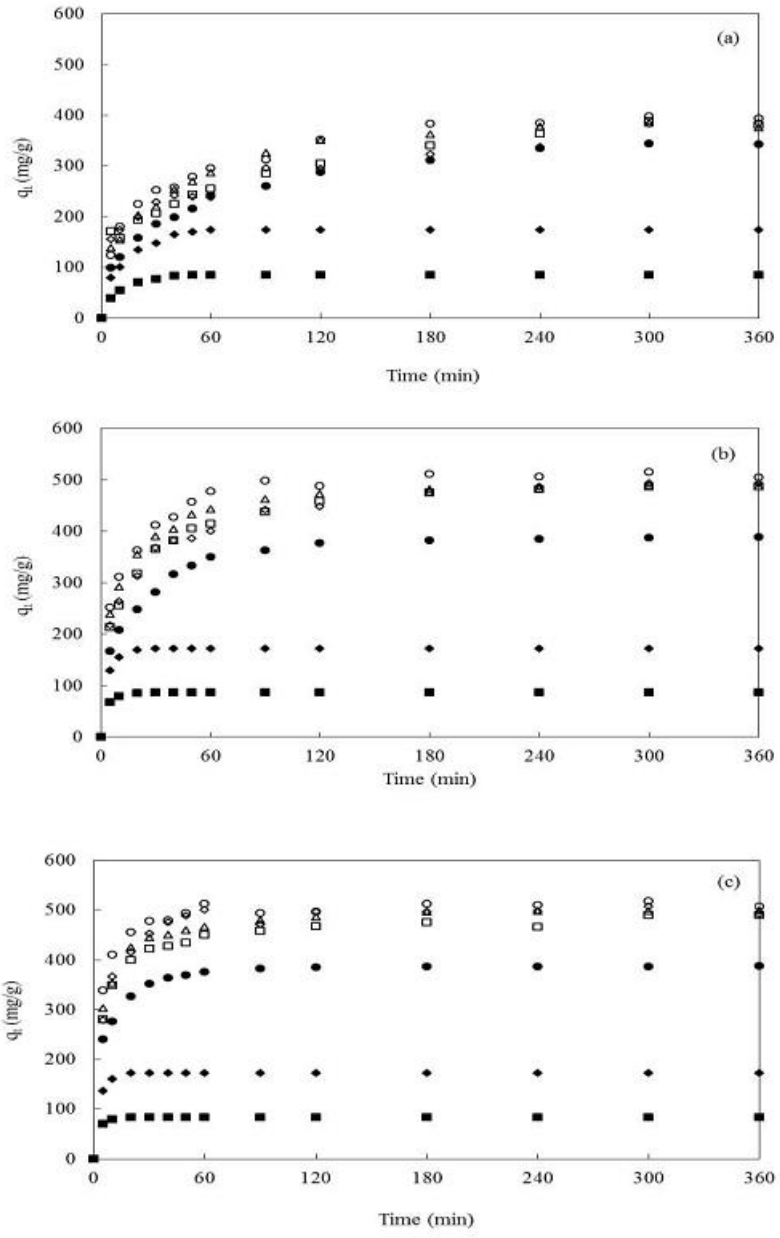
(a)
(b)
(c)
q_t (mg/g)
Time (min)
0
60
120
180
240
300
360
100
200
300
400
500
600

Fig. 8

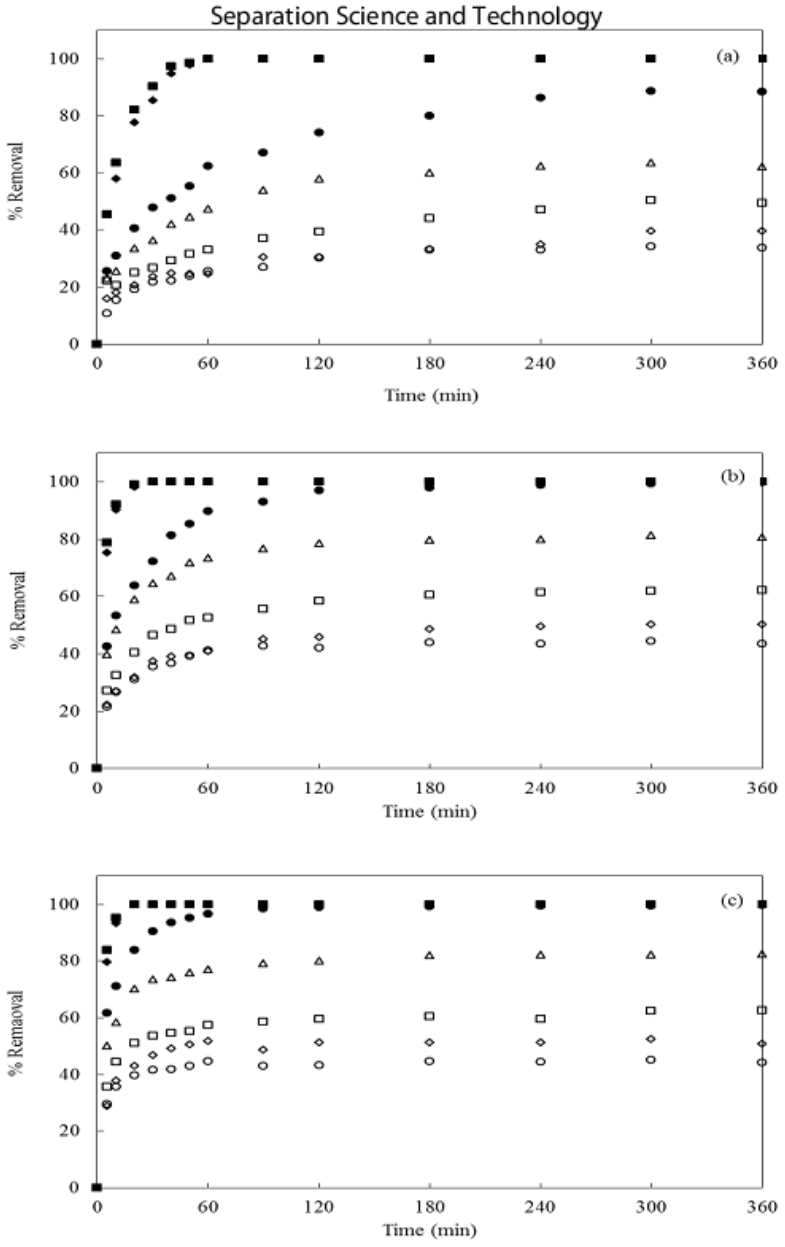
Separation Science and Technology
(a)
(b)
(c)
% Removal
% Remaoval
Time (min)
0
20
40
60
80
100
0
60
120
180
240
300
360

Fig. 9

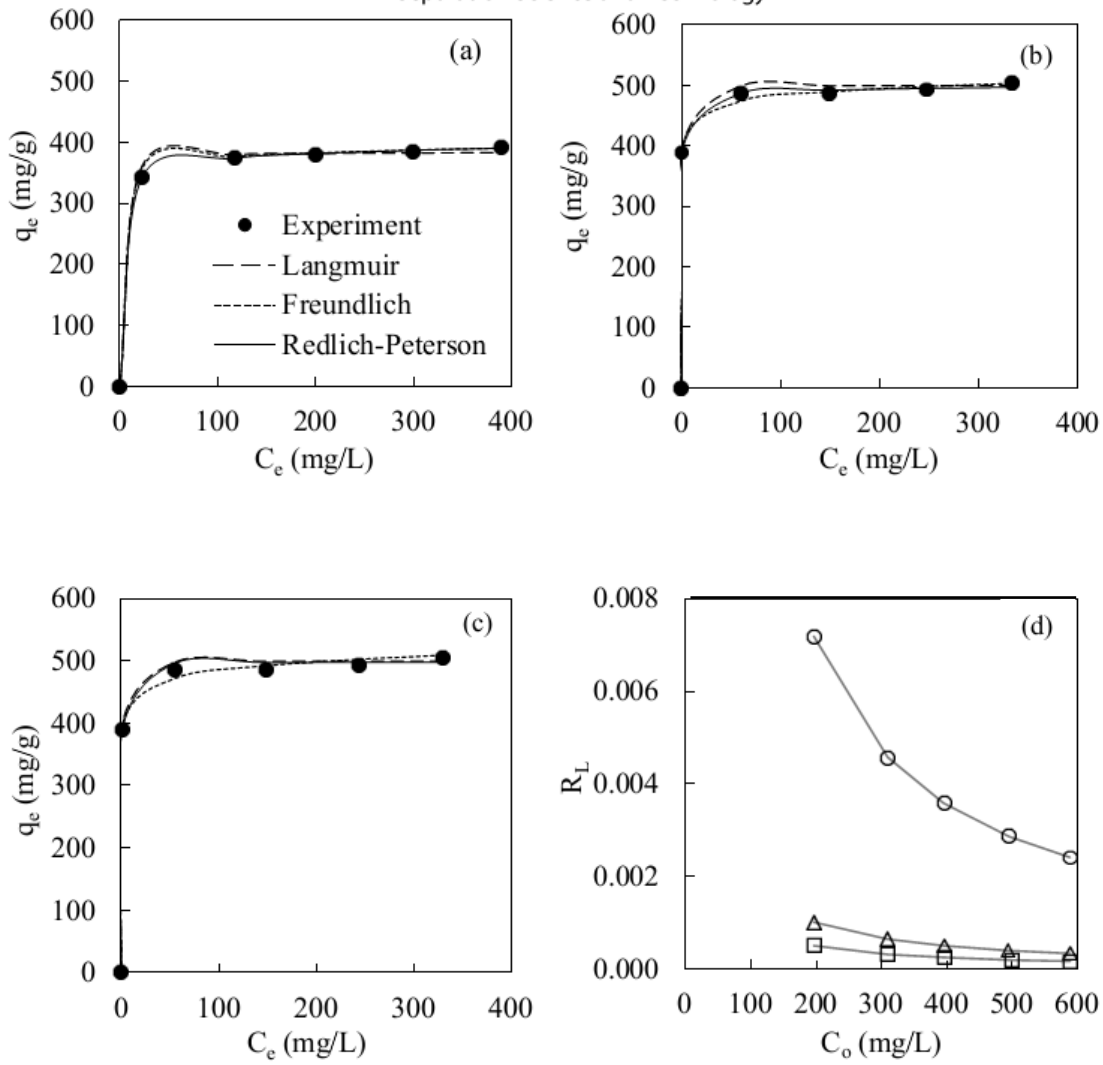
(a)
(b)
(c)
(d)
Experiment
Langmuir
Freundlich
Redlich-Peterson
q_e (mg/g)
C_e (mg/L)
R_L
C_o (mg/L)

Fig. 10

ประวัตินักวิจัยและคณะ พร้อมหน่วยงานสังกัด

หัวหน้าโครงการ ศาสตราจารย์ ดร.เหมือนเดือน พิศาลพงศ์

ส่วนงาน ภาควิชาวิศวกรรมเคมี คณะวิศวกรรมศาสตร์

คุณวุฒิ Ph.D. (Chemical Engineering) Colorado State University, พ.ศ. 2542

ผลงานทางวิชาการด้าน บทความวิชาการ, ตำรา/หนังสือ

บทความวิชาการ (ปี 2554 – ปัจจุบัน)

1. Bangrak, P., Limtong, S., Phisalaphong, M., “Continuous ethanol production using immobilized yeast cells entrapped in loofareinforced alginate carriers”, Brazilian Journal of Microbiology Vol. 42, p 676-684 (2011).

2. Mongkolkajit, J., Pullsirisombat, J., Limtong, S., Phisalaphong, M., “Alumina-doped alginate gel as a cell carrier for ethanol production in a packed-bed bioreactor”, Biotechnology and Bioprocess Engineering Vol.16, p 505-512 (2011).

3. Chiaoprakobkij, N., Sanchavanakit, N., Subbalekha, K., Pavasant, P., Phisalaphong, M., “Characterization and biocompatibility of bacterial cellulose/alginate composite sponges with human keratinocytes and gingival fibroblasts”, Carbohydrate Polymers Vol.85, p 548-553 (2011).

4. Rattanapan, A., Limtong, S., Phisalaphong, M., “Ethanol production by repeated batch and continuous fermentations of blackstrap molasses using immobilized yeast cells on thin-shell silk cocoons”, Applied Energy Vol.88, p 4400-4404 (2011).

5. Eiadpum, A., Limtong, S., Phisalaphong, M., “High-temperature ethanol fermentation by immobilized coculture of Kluyveromyces marxianus and Saccharomyces cerevisiae”, Journal of Bioscience and Bioengineering Vol.114, p 325-329 (2012).

6. Taokaew, S., Seetabhawang, S., Siripong, P., Phisalaphong, M., “Biosynthesis and characterization of nanocellulose-gelatin films”, Materials Vol.6, p 782-794 (2013).

7. Phisalaphong, M., Kirdponpattara, S., Kingkaew, J., Taokaew, S., Chiaoprakobkij, N., Sanchavanakit, N., “Modification of bacterial cellulose by adding interfering biopolymers", Abstracts of papers of the American Chemical Society, Vol. 245 Meeting Abstract: 123-CELL Published: 7 April 2013.

8. Taokaew, S., Phisalaphong, M., Yin, LY, Newby, BMZ. Effects of drying methods of bacterial cellulose membrane on differentiation and proliferation of induced pluripotent stem cells, Abstracts of papers of the American Chemical Society, Volume: 245 Meeting Abstract: 102-CELL Published: 7 April 2013.

9. Kirdponpattara, S., Phisalaphong, M., Newby, B.M.Z., "Applicability of Washburn capillary rise for determining contact angles of powders/porous materials", Journal of Colloid and Interface Science Vol.397, p 169-176, (2013) .

10. Kirdponpattara, S., Phisalaphong, M., "Bacterial cellulose-alginate composite sponge as a yeast cell carrier for ethanol production", Biochemical Engineering Journal, 77, p 103-109 (2013).

11. Kirdponpattara, S., Newby, B.Z., Phisalaphong, M., "Effect of oxygen plasma treatment on bacterial cellulose-alginate composite sponge as a yeast cell carrier for ethanol fermentation", Advanced Materials Research, 724-725, pp. 1150-1153 (2013).

12. Mulalee, S., Chanprasert, J., Kerdpoksup, P., Sawangpanya, N.S., Phisalaphong, M. "Esterification of oleic acid and bioalcohols using immobilized lipase", Advanced Materials Research, 724-725, p 1154-1157 (2013).

13. Taokaew, S., Phisalaphong, M., Zhang Newby, B.-M., "In vitro behaviors of rat mesenchymal stem cells on bacterial celluloses with different moduli", Materials Science and Engineering C, Vol.38, p 263-271 (2014).

14. Taokaew, S., Nunkaew, N., Siripong, P., Phisalaphong, M., "Characteristics and anticancer properties of Bacterial cellulose films containing ethanolic extract of mangosteen peel", Journal of Biomaterials Science: Polymer Edition Vol. 25(9), p. 907-922 (2014).

15. Kingkaew, J.,Kirdponpattara, S.,Sanchavanakit, N.,Pavasant, P., Phisalaphong, M., "Effect of Molecular Weight of Chitosan on Antimicrobial Properties and Tissue Compatibility of Chitosan-impregnated Bacterial Cellulose Films", Biotechnology and Bioprocess EngineeringVol.19(3), p 534-544 (2014).

16. Mulalee, S., Sena, K., Phisalaphong, M., "Enzymatic esterification of oleic acid and propanol by Novozym 435", Applied Mechanics and Materials Vol.705, p 29-33 (2015).

17. Kittithanesuan, N., Phisalaphong, M., "Thin-shell silk socoon (TSC) as a nitrogen source of ABE fermentation by Clostridium acetobutylicum", Applied Mechanics and Materials Vol.705, p14-18 (2015).

18. Kittithanesuan, N., Phisalaphong M. “Enhanced acetone-butanol production from sugarcane juice by immobilized Clostridium acetobutylicum (ATCC 824) on thin-shell silk cocoons”, Biotechnology and Bioprocess Engineering Vol. 20 (3), p 599-607(2015).

19. Suratago, T., Taokaew, S., Kanjanamosit, N., (...), Burapatana, V., Phisalaphong, M. “Development of bacterial cellulose/alginate nanocomposite membrane for separation of ethanol-water mixtures” Industrial and Engineering Chemistry Vol. 32, p 305-312 (2015).

20 Taokaew, S., Phisalaphong, M., Zhang Newby, B.-M., “Modification of bacterial cellulose with organosilanes to Improve attachment and spreading of human fibroblasts”, Cellulose Vol. 22 (4), p 2311-2324, (2015).

21. Kirdponpattara, S., Khamkeaw, A., Sanchavanakit, N., Pavasant, P., Phisalaphong, M. “Structural modification and characterization of bacterial cellulose-alginate composite scaffolds for tissue engineering”, Carbohydrate Polymers Vol.132 p. 146-155 (2015).

22. Mulalee, S., Srisuwan, P., Phisalaphong, M., “Influences of operating conditions on biocatalytic activity and reusability of Novozym 435 for esterification of free fatty acids with short-chain alcohols: a case study of palm fatty acid distillate (PFAD)”, Chinese Journal of Chemical Engineering Vol.23 p.1851–1856 (2015).

23. Khamkeaw, A., Phisalaphong, M., “Hydrolysis of cassava starch by co-immobilized multi-microorganisms of Loog-Pang (Thai rice cake starter) for ethanol fermentation”, Food Science and Biotechnology Vol. 25(2), p. 509-516 (2016).

24. Suratago, T., Panitchakarn, P., Kerdlarpphon, P., Burapatana, V., Phisalaphong, M. “Bacterial cellulose-alginate membrane for dehydration of biodiesel-methanol mixtures” Engineering Journal Vol. 20(5), p. 145-153 (2016)

25. Phomrak, S., Phisalaphong, M., “Reinforcement of Natural Rubber with Bacterial Cellulose via a Latex Aqueous Microdispersion Process”, Journal of Nanomaterials, 4739793 (2017).

26. Ibnu Abdulwahab, M.., Khamkeaw, A., “Jongsomjit, B., Phisalaphong, M. “Bacterial Cellulose Supported Alumina Catalyst for Ethanol Dehydration”, Catalysis Letters Vol. 147(9), p. 2462-2472 (2017)

27. Kirdponpattara, S., Phisalaphong, M., Kongruang, S. “Gelatin-bacterial cellulose composite sponges thermally cross-linked with glucose for tissue engineering applications”, Carbohydrate Polymers Vol. 177, pp. 361-368 (2017)

28. Taokaew, S., Piyaviriyakul, S., Siripong, S., Phisalaphong, M. “Aqueous and Ethanolic Extracts of Mangosteen Peels as Natural Antimicrobial/anticancer Materials Against Pathogenic Microbes and B16F10 Murine Melanoma”, Chiang Mai J. Sci. 2017 (in press)

ตำรา/หนังสือ (Book Chapter) (ปี 2554 – ปัจจุบัน)

1. Taokaew, S., Phisalaphong, M., Newby, B.-M.Z. Bacterial cellulose: Biosyntheses, modifications, and applications in Applied Environmental Materials Science for Sustainability. Ed. by T. Kobayashi 2016, IGI Global (Hershey, PA 17033, USA).

2. Phisalaphong, M., Tran, T-K, Taokaew, S., Budiraharjo, R., Febriana, G, Nguyen, D-N, Chu-Ky, S., Dourado, F., Nata de coco Industry in Vietnam, Thailand, and Indonesia, in Bacterial Nanocellulose: From Biotechnology to Bio-Economy, Ed. by M. Gama, F. Dourado, S. Bielecki 2016, Elsevier (B.V., Amsterdam, The Netherland).

3. Phisalaphong, M., Kirdponpattara, S., Synthesis and Characterization of Bacterial Cellulose-Based Composites and Their Applications, Handbook of Sustainable Polymers: Processing and Applications. Ed. by V. K. Thakur and M. K. Thakur, 2015, Pan Stanford Publishing Pte. Ltd. (Singapore).

4. Phisalaphong, M., Chiaoprakobkij, N., Applications and Products-Nata de Coco, in Bacterial NanoCellulose; a sophisticated multifunctional material. Ed. by M. Gama, P. Gatenholm and D. Klemm, 2013, CRC Press, Taylor & Francis Group (Florence, KY, USA).

5. Phisalaphong, M.,Jatupaiboon, N., Kingkaew, J., Biosynthesis of Cellulose-Chitosan Composite, in Chitin, Chitosan, Oligosaccharides and Their Derivatives. Ed. By Se-Kwon Kim, 2011, CRC Press, Taylor & Francis Group (Florence, KY, USA).